



THE UNIVERSITY *of* EDINBURGH

Edinburgh Research Explorer

## **Screening the Geomechanical Stability (Thermal & Mechanical) of Shared Multi-user CO<sub>2</sub> Storage Assets, a Simple Effective Tool Applied to the Captain Sandstone Aquifer**

**Citation for published version:**

McDermott, C, Williams, J, Tucker, O, Jin, M, Mackay, E, Edlmann, K, Haszeldine, RS, Wang, W, Kolditz, O & Akhurst, M 2016, 'Screening the Geomechanical Stability (Thermal & Mechanical) of Shared Multi-user CO<sub>2</sub> Storage Assets, a Simple Effective Tool Applied to the Captain Sandstone Aquifer' International Journal of Greenhouse Gas Control, vol. 45, pp. 43-61. DOI: 10.1016/j.ijggc.2015.11.025

**Digital Object Identifier (DOI):**

[10.1016/j.ijggc.2015.11.025](https://doi.org/10.1016/j.ijggc.2015.11.025)

**Link:**

[Link to publication record in Edinburgh Research Explorer](#)

**Document Version:**

Peer reviewed version

**Published In:**

International Journal of Greenhouse Gas Control

**General rights**

Copyright for the publications made accessible via the Edinburgh Research Explorer is retained by the author(s) and / or other copyright owners and it is a condition of accessing these publications that users recognise and abide by the legal requirements associated with these rights.

**Take down policy**

The University of Edinburgh has made every reasonable effort to ensure that Edinburgh Research Explorer content complies with UK legislation. If you believe that the public display of this file breaches copyright please contact [openaccess@ed.ac.uk](mailto:openaccess@ed.ac.uk) providing details, and we will remove access to the work immediately and investigate your claim.



# 1 Screening the Geomechanical Stability (Thermal & Mechanical) of 2 Shared Multi-user CO<sub>2</sub> Storage Assets, a Simple Effective Tool Applied 3 to the Captain Sandstone Aquifer 4

5 \*Christopher McDermott<sup>1</sup>, John Williams<sup>2</sup>, Owain Tucker<sup>3</sup>, Min Jin<sup>4</sup>, Eric Mackay<sup>4</sup>, Katriona Edlmann<sup>1</sup>,  
6 R. Stuart Haszeldine<sup>1</sup>, Wenqing Wang<sup>6</sup>, Olaf Kolditz<sup>6</sup>, Maxine Akhurst<sup>5</sup>

7 \*Corresponding author [christopher.mcdermott@ed.ac.uk](mailto:christopher.mcdermott@ed.ac.uk)

8 <sup>1</sup>University of Edinburgh, School of Geosciences, Edinburgh, UK

9 <sup>2</sup>British Geological Survey, Keyworth, Nottingham, UK

10 <sup>3</sup>Shell Projects & Technology, Aberdeen, UK.

11 <sup>4</sup>Heriot-Watt University, Institute of Petroleum Engineering, Edinburgh, UK

12 <sup>5</sup>British Geological Survey, Edinburgh, UK.

13 <sup>6</sup>Helmholtz Center for Environmental Research, Leipzig, Germany.

## 14 15 Abstract

16 Multi-user stores are anticipated in the near future to permanently store CO<sub>2</sub> captured at industrial  
17 sources to meet emissions reductions targets. Multiple storage permit applications will be required  
18 to exploit the immense potential capacity within extensive CO<sub>2</sub> storage assets. To retain 99% of the  
19 injected CO<sub>2</sub> for 1000 years the geomechanical stability of the sealing strata above the pressurised  
20 storage reservoir is a key factor which needs to be included in the geo-engineering design of shared  
21 storage assets. The potential for interaction of increased pressure at multiple injection sites needs to  
22 be predicted and assessed at a regional scale to assure the integrity at all existing sites before a  
23 storage permit is granted. Geomechanical models coupled with the expected fluid pressure response  
24 predict the stability of the storage asset during and after injection of CO<sub>2</sub> at multiple injection sites,  
25 and can be used as a tool to ensure efficient utilisation of the storage capacity. The geomechanical  
26 analysis of the thermal stress as well as local and regional fluid pressure changes requires a detailed  
27 numerical evaluation, often at a resolution significantly higher than the data available. Coupling of  
28 regional-scale static geological models, dynamic multi-phase flow models and detailed  
29 geomechanical models requires extensive computational resources. Such models often produce  
30 seemingly detailed results, but are usually only one or two realisations of a system populated by a  
31 statistically generated parameter set. Limits on time and computational resources prevent more  
32 simulations within fixed time and financial budgets. To enable a more time and cost efficient  
33 methodology of assessing the geomechanical stability of potential storage sites we present a four-  
34 tier modelling approach with increasing complexity that allows an in-depth evaluation of the  
35 geomechanical stability at a regional scale of a multi-user storage asset taking into account the fluid  
36 pressure increase and the thermal stress impact on the stability of the strata sealing the CO<sub>2</sub> store.  
37 The tiers include (1) development of a geo-mechanical facies model of the storage system, (2)  
38 development of an analytical geomechanical model for the storage site static stress conditions, (3)  
39 fitting an empirical multivariable polynomial function to the analytical model, and (4) conditioning  
40 the empirical function using coupled numerical THM modelling for dynamic stress conditions. The  
41 result is a look up function which gives the maximum possible fluid pressure as a function of location.  
42 This approach significantly simplifies the computational requirements and time for the prediction of  
43 geomechanical behaviour. In addition to presenting this methodology, using the Captain Sandstone  
44 of the North Sea as an example, three key findings are further examined. Firstly, detailed analysis of

45 the stress changes as a result of cold fluid injection suggests that the redistribution of thermal stress  
46 can, in some cases, be beneficial to the storage system depending on the stress bridging which  
47 occurs. Secondly, pressure plume migration over time in dipping strata, from deeper injection sites  
48 to shallower sites, needs to be taken into account. Thirdly, the nature of the strata underlying the  
49 storage formation is critical to the pressure increase in response to the fluid injection. The  
50 methodology developed in this paper enables a rapid and efficient screening of the dynamic  
51 geomechanical stability and an efficient coupling to diverse discrete multiphase fluid flow models  
52 using commonly available computational resources.

### 53 Key Words

54 Geomechanical simulation, scCO<sub>2</sub> storage, Reservoirs, Rock mechanics, THM numerical modelling,  
55 Screening tool

### 56 Introduction

57 Carbon capture and storage permanently stores CO<sub>2</sub> captured at large-scale industry and power  
58 plants to significantly reduce the emission of anthropogenic waste CO<sub>2</sub> to the atmosphere, and  
59 address one of the key concerns regarding global climatic change. Sovereign countries and  
60 competent authorities that possess and regulate large commercially attractive offshore resources  
61 are increasingly aware of the need to manage the storage of CO<sub>2</sub>. Such storage resource assets need  
62 to be managed with a joined-up approach, and not just an unsustainable exploitation of ‘what is  
63 possible and cheapest now’, to optimise potential storage capacity. Failure to do so could lead to a  
64 reduction in the usable storage capacity, due to store integrity constraints, and significant long term  
65 deterioration in the asset value. The challenge will increase where the strata used for multiple  
66 injection sites extend across international borders.

67 Given the extent of regional storage formations, it is expected that multiple injection sites will  
68 operate to exploit the same contiguous and hydraulically connected pore space. Competition for the  
69 storage capacity asset should be expected; without effective pressure management even relatively  
70 small volumes of stored CO<sub>2</sub> can have a significant impact on the regional fluid pressure within the  
71 storage formation. Additionally, the maximum acceptable pressure values predicted by geo-  
72 mechanical modelling do not display a linear relationship with the depth of the storage formation. In  
73 dipping strata long-term migration of increased pressure to shallow areas, which may be at some  
74 distance from the CO<sub>2</sub> injection points, may determine the maximum acceptable pressure at deeper  
75 parts of the formation.

76 In this paper a generic methodology is presented enabling the geomechanical stability of a storage  
77 site to be relatively rapidly assessed at a regional scale. The methodology develops a “look up”  
78 function (location dependent) enabling geomechanical pressure limits to be transferred simply from  
79 one simulator to another. The methodology is developed on and applied to the Captain Sandstone in  
80 the North Sea (Figures 1 and 2) (Kopervik Fairway of Law et al., 2000). This is assessed as a potential  
81 multi-user store as it is a preferred site for a UK demonstrator project for geological CO<sub>2</sub> storage  
82 (DECC, 2013). The geomechanical impact of the injection of commercially viable storage volumes of  
83 dense supercritical (sc) phase CO<sub>2</sub> into the Captain Sandstone was investigated at two realistic  
84 locations: Site A in the vicinity of the Goldeneye Gas Field; Site B in brine-saturated Captain  
85 Sandstone approximately forty kilometres up-dip of Site A (Figure 1).

86 Predictive modelling of potential pressure changes within the storage formation to ensure  
87 prospective storage operations are within the acceptable geomechanical limits requires the use of  
88 numerical multi-physics models. Such models enable assessment the efficient utilisation of the  
89 available storage capacity. These models require reliable geological, fluid flow and geomechanical  
90 information. Information is needed on a regional scale for the strata present, and this needs to be  
91 discretised to sufficient detail that reasonable geometrical models of the injection sites can be

92 constructed, and an acceptable parameterisation of the strata undertaken. The parameterisation  
93 needs to address all the values required for the multi-physics simulation of the system.

94 There are several simulators, and combination of codes, that allow simultaneous evaluation of the  
95 fluid flow and the geomechanical response, e.g. Magri et al. (2013), Rutqvist et al. (2006), Rutqvist et  
96 al. (2002). However multi-physics problems generally require data at several different scales of  
97 resolution, particularly where discrete features such as faults in the geomechanical analysis are  
98 taken into account e.g. Cappa and Rutqvist (2011), Vidal-Gilbert et al. (2009). The scale and  
99 availability of data required in the different simulations means that efficient methods are required to  
100 integrate the results of one part of the simulation with another.

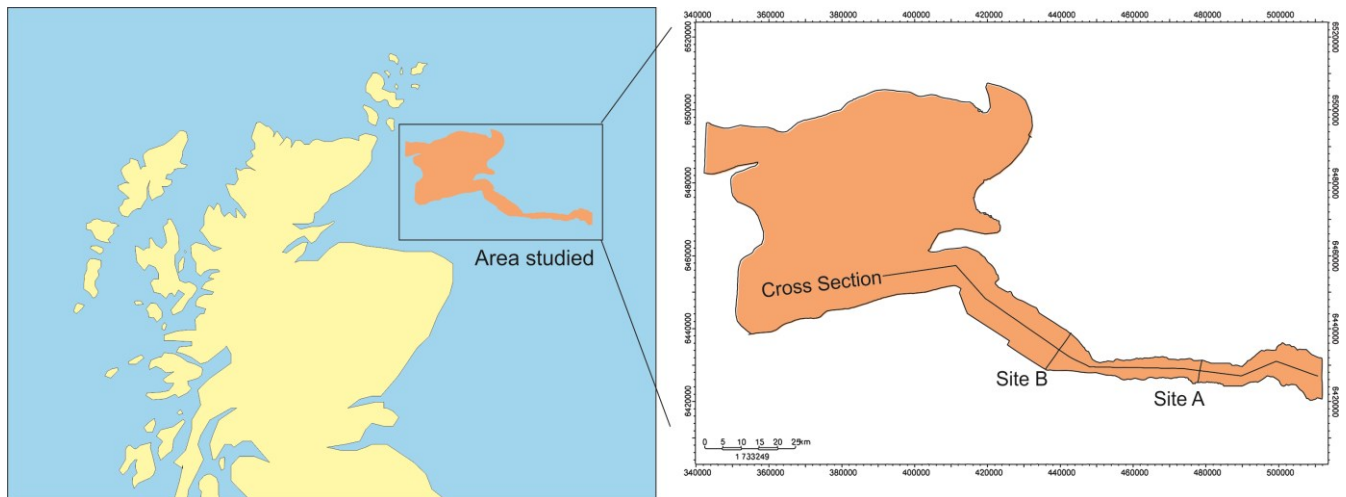
101 The geomechanical modelling requires both detailed representation of the area around the injection  
102 wells where the impact of the thermal signal is to be taken into account, and also a regional  
103 representation of the strata to account for the large areal extent of a possible pressure increase. In  
104 this study the impact of the thermal stress around the injection well was evaluated using a grid size  
105 of the order of a few metres, whereas the geological heterogeneity recorded in the horizontal  
106 dimension within the storage formation was approximately 250 metres.

107 Parameterisation of numerical models of regional extent is usually based upon a statistical approach  
108 with data taken from relatively few selected boreholes. The resolution achieved here of 250 metres  
109 is more finely scaled than usually available, which is normally in the order of 500 metres or more.  
110 The data is typically presented as a probability distribution function rather than a true kriged  
111 statistical analysis as there is not sufficient confidence in the evaluation of the correlation of the  
112 parameters with geometrical location. A normal, or log normal, distribution approach to the  
113 evaluation of the material characteristics can be expected to capture the behaviour of the system as  
114 a whole. However, any single realisation of the statistical field is just one representation of a wide  
115 range of equally valid possibilities. Usually, modelling is constrained by the computational power and  
116 time needed to run multiple simulations.

117 Here we present a four-tier modelling approach, applied to the Captain Sandstone offshore  
118 Scotland, to evaluate the geomechanical stability of a multi-user store to CO<sub>2</sub> injection as a  
119 consequences of multiple sites of injection, covering both thermal effects near the well and regional  
120 pressure build up. The tiers include (1) development of a geo-mechanical facies model of the storage  
121 system, (2) development of an analytical geomechanical model for the storage site static stress  
122 conditions, (3) fitting an empirical multivariable polynomial function to the analytical model, and (4)  
123 conditioning the polynomial function using coupled numerical THM modelling for dynamic stress  
124 conditions along a number of cross sections. Tier (4) results in a depth, and where relevant, location,  
125 dependent look up function which is easily transferable to other simulators.

126 Three key findings are also examined here. Firstly, detailed analysis of the stress changes as a result  
127 of cold fluid injection which suggests that the redistribution of thermal stress can, in some cases, be  
128 beneficial to the storage system depending on the stress bridging which occurs. Secondly, pressure  
129 plume migration in dipping strata from deeper injection sites to shallower sites over time needs to  
130 be taken into account. Thirdly the nature of the strata underlying the storage formation is critical to  
131 the pressure increase in response to CO<sub>2</sub> injection.

132



133  
 134 **Figure 1** Location of Captain Sandstone offshore Scotland, northern North Sea (left) and extent of area studies (inset  
 135 right).

136 **Method**

137 The geomechanical modelling is of a volume of the Captain Sandstone where it is narrowed and is  
 138 termed the Captain Sandstone Fairway, indicated by the location of the cross-section in Figure 1. We  
 139 develop a four tier modelling approach of increasing complexity to the evaluation of the  
 140 geomechanical stability of the Captain Sandstone Fairway during the proposed injection of the CO<sub>2</sub>.  
 141 The result is a portable empirical function based on detailed geomechanical modelling which can be  
 142 used to predict maximum possible safe fluid pressures within the Captain Sandstone Fairway.

- 143 • Tier 1: Development of a conceptual geomechanical facies model
- 144 • Tier 2: Development of an analytical geomechanical model for static conditions
- 145 • Tier 3: Fitting Tier 2 with an empirical polynomial function
- 146 • Tier 4: Application of 2D and 3D multi-physics coupled process models to refine the Tier 3 polynomial  
 147 function to include dynamic stress conditions and resulting in the location dependent look up function.

148 The result from Tier 4 is a spatially correlated estimation of the maximum overpressure possible  
 149 within the storage strata, including both the reservoir (principal storage location), primary seal and  
 150 secondary seal. Each of these Tiers are described here and discussed in more detail later.

151 The first Tier comprises assessing the geological information on the storage complex (as defined in  
 152 EU, 2011) and developing a geomechanical facies model of the system. The geomechanical facies  
 153 model provides the basis for the further modelling investigation and parameterisation of the system  
 154 (Edlmann et al. 2014; McDermott et al. 2006a; Tenzer et al. 2010).

155 The second Tier uses an analytical approach for static stress conditions prior to dense phase CO<sub>2</sub>  
 156 injection to evaluate maximum fluid pressures possible in the storage complex. The analytical  
 157 modelling provides a generic approach to the evaluation of the stability of a rock unit as a function  
 158 of the poly axial stress, fluid pressure and rock mechanical parameters. Possible failure mechanisms  
 159 of the rock at this level include tensile failure, shear failure and reactivation of existing planes of  
 160 weakness. At this level as much available data as possible is included in terms of stress profile from  
 161 field measurements and laboratory results of solid, fluid and medium properties. The analytical  
 162 solution provides a reference value for the maximum fluid pressures which can be contained, but  
 163 does not take into account local heterogeneity (different thicknesses of strata, parameter  
 164 variations), the impact of thermal stress or the dynamic impact of the increase in the fluid pressure  
 165 and consequent reduction in horizontal stress within the storage complex.

166 The third Tier is to develop an empirical multivariable polynomial function which provided the  
 167 maximum possible fluid pressure in the storage complex predicted by Tier 2 as function of depth and

168 location (primary seal, secondary seal or faulting). This was refined in Tier 4 to include the dynamic  
169 stress conditions, heterogeneity and thermal stress.

170 The forth Tier of evaluation was to employ fully coupled thermal hydraulic mechanical (THM) multi-  
171 physics code at a number of selected locations throughout the Captain Sandstone. The coupled  
172 process finite element simulator, OpenGeosys, (Kolditz et al. 2012) was further developed to include  
173 standard rock mechanical stability analysis. This was then used to simulate a large scale 3D model  
174 (HM), approximately 130 by 20 kilometres, and selected high resolution 2D (THM) cross sections  
175 (mesh resolution to ten metres) to evaluate the maximum safe dynamic fluid pressure in the Captain  
176 Sandstone. The 3D model provided realistic estimates of the changes in fluid pressure expected  
177 during the injection of commercial-scale volumes of CO<sub>2</sub> (6million tonnes (Mt) per year at each site).  
178 The predicted fluid changes in the 3D model were then used to define the source terms and pressure  
179 changes expected in the 2D detailed resolution models (2D THM). The same failure mechanisms  
180 included in the Tier 2 model were included in the 2D THM numerical models. These models enabled  
181 local heterogeneity in terms of the different thicknesses of strata to be included, the impact of  
182 thermal stress to be assessed and the dynamic impact of the increase in the fluid pressure and  
183 reduction in horizontal stress to be taken into account.

184 The results of the third Tier empirical function were then compared with the results of the forth Tier  
185 dynamic THM modelling results. The empirical function was refined with a correction factor to  
186 match the fourth Tier results, i.e. include the dynamic modelling results. The correction factor could  
187 also takes into account the location in terms of defining a zone of possible influence of the thermal  
188 stress around the injection sites, the presence of fault zones and which strata the analysis was in  
189 (primary seal, secondary seal). The augmented empirical fit then provides a depth and location  
190 dependent maximum safe fluid pressure throughout the Captain Sandstone Fairway and sealing  
191 strata. This function can then be ported to be used in detailed multiphase fluid pressure simulations  
192 as a simple look up function approach providing coverage for the whole of the Captain Sandstone  
193 Fairway. The depth and location dependent function provides a numerical summary of the detailed  
194 geomechanical simulations.

## 195 Model assumptions

196 A modelling approach provides a mathematical approximation of reality and a tool for estimating the  
197 behaviour of the system based on known processes. Simplification of the system needs to be  
198 undertaken whereby the main processes operating are captured. The model requires simplifications  
199 in terms of the geometry of the deposits, the range of parameters assigned to the deposits, the  
200 discretisation of the heterogeneities both within strata and between strata, the fluid properties, and  
201 the processes to be included. In précis four assumptions on the behaviour of the system were  
202 applied to simplify the modelling approach;

203 Assumption 1: Fluid flow and pressure build up can be satisfactorily modelled as single-phase flow.  
204 This assumption was based on the facts that the reservoir temperature is of the order of 83 °C in the  
205 storage asset, and so the viscosity of brine at this temperature is approximately 0.0004 Pa s. scCO<sub>2</sub>  
206 injected at 20°C has a viscosity of circa 0.0001 Pa s. Therefore, the overall control on the pressure  
207 build up around the injection well will be that of the mobility of the far-field brine and not the CO<sub>2</sub> in  
208 the vicinity of the well. Thermal calculations show that a significant temperature effect generated by  
209 CO<sub>2</sub> injection is localised to <1km after 30 years. The advantage that this assumption has is that a  
210 multiphase flow simulation would require significantly more computational resources, as well as  
211 several further parametrical modelling assumptions such as capillary entry pressures, relative  
212 permeability curves and hysteresis behaviours of wetting and non-wetting fluids. Therefore this  
213 assumption significantly simplifies the computational resource required.

214 Assumption 2: The model was populated with mean parameters for strata layers and the layers  
215 considered to be homogeneous and isotropic. This approach was based on the nature of the data  
216 available. The grid spacing of geometrical and geological data was resolved down to 250m

217 horizontally, and metre-scale vertically. The geometry and structure of the strata were taken from  
218 cross-sections from the static geological CO<sub>2</sub>MultiStore Captain Sandstone model (Figure 1). The  
219 heterogeneity of the different layers is known stochastically and not discretely.

220 Assumption 3: The mechanical response of the system was modelled for elastic conditions only.  
221 Plastic deformation was not considered.

222 Assumption 4: Fluid flow out of the model may occur within the Captain Sandstone Fairway to the  
223 south east and north west, it does not occur to adjacent lateral strata, it may or may not occur  
224 through the base of the underlying strata. Identifying realistic boundary conditions (for both the  
225 hydraulic and the mechanical model) is key to successfully calibrating the modelling approach. In  
226 general, the lateral boundaries of the Captain Sandstone Fairway were considered to be closed to  
227 fluid flow as the geology showed there was no extension of the Captain Sandstone beyond the limits  
228 of the Fairway. The lateral boundaries were also assumed to be ridged. This was based on the fact  
229 that there was little information available on the nature of the material beyond the boundaries of  
230 the Captain Fairway and it was clear that an assumption of unrestrained boundaries was not valid.  
231 Assuming ridged lateral boundaries, so that any lateral boundary deformation is not accommodated  
232 by strain, leads to a worst case assumption in terms of stress build up, but therefore a safer analysis  
233 of the impact on the integrity of the strata due to possible overpressure build up due to CO<sub>2</sub> injection  
234 in the strata. The base of the model was considered immobile. The top surface was considered open  
235 to fluid flow, at constant temperature and able to deform.

236 One of the most important assumptions proved to be the type of fluid flow boundary for the base of  
237 the model. Two boundaries types were considered to give “end member” results. First at the base of  
238 the model an open flow boundary was considered where the pressure release from the model  
239 through the base was dictated by a layer of strata circa 800 metres thick with a permeability  
240 representative of this strata, and secondly a no flow fluid boundary at the base of the model.

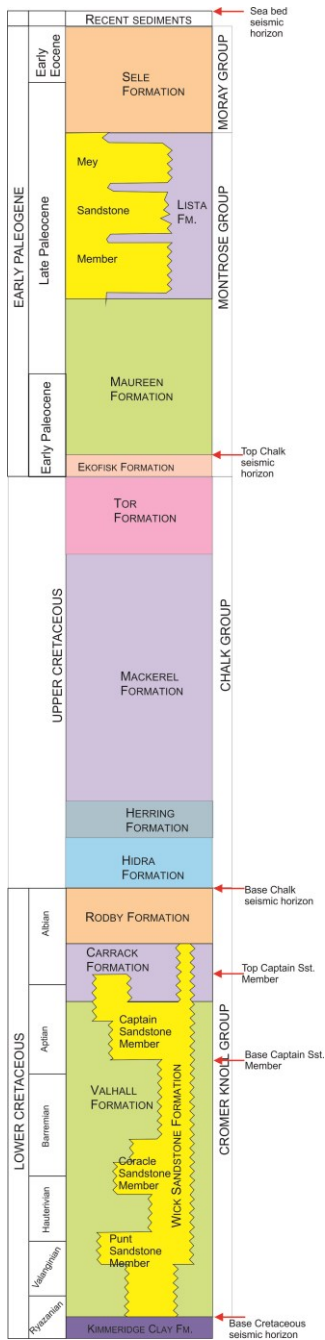
241 The choice of the base of the model as a constant hydrostatic fluid pressure boundary allows excess  
242 pressure in the reservoir to be released through the under lying strata (the Underburden). The  
243 Underburden defined in the geomechanical model comprises a stratigraphic sequence of  
244 sedimentary deposits including mudstone and sandstone down to strata of Permian age. The  
245 Jurassic sequence comprises the Kimmeridge Clay and sandstone, beneath which are volcanic rocks.  
246 These are underlain by mudstone and sandstone of Triassic age that overlie strata of Permian age  
247 marked by evaporate deposits of the Zechstein Group. This Jurassic to Permian sequence can be  
248 several kilometres in thickness, and only at the Zechstein evaporite deposits can we be sure that  
249 there is a no-flow boundary. Choosing the base of the model to be impermeable means that the  
250 pressure release from injection into the sandstone can only occur either through the seal rocks or  
251 through the open edges of the model (farther north westwards and farther south eastwards where  
252 the Captain Sandstone Fairway is known to extend further). The assumption of the lower boundary  
253 of the Underburden being closed to flow leads to significantly higher pressures being built up in the  
254 reservoir than if the lower boundary of the underburden allows some pressure release. In addition it  
255 leads to increased pressure communication between the separate injection sites.

## 256 **Tier 1: From geology to geomechanical facies**

257 A brief overview of the geology of the Captain Sandstone Fairway is presented as a stratigraphic  
258 column in Figure 2. A cross section of the Captain Sandstone Fairway is presented in Figure 3, the  
259 location of the cross section is illustrated in Figure 1. The uppermost strata comprise the recent  
260 deposits of the Nordland Group, underlain by Tertiary strata of the Moray Group and the Montrose  
261 Group. These are variously inter-bedded cohesive and non-cohesive units, with a thickness in the  
262 Captain Sandstone Fairway of several hundreds of metres. At the base of the Cenozoic deposits the  
263 youngest chalk interval is the Ekofisk Formation. The Upper Cretaceous succession comprises the  
264 Tor, Mackerel and Herring formations. Within this group there are occasional mudstone units which

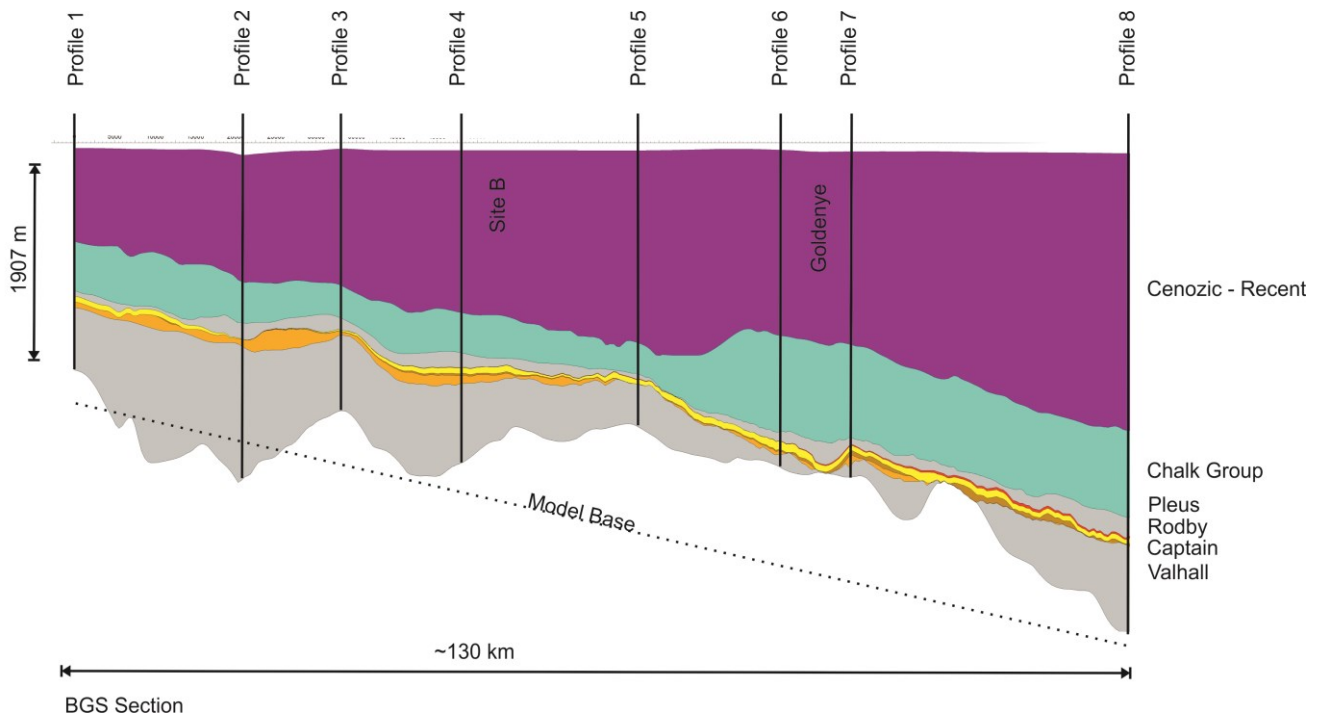
265 are considered to be sealing. These are found towards the east of the Captain Sandstone Fairway,  
266 with a thickness of the order of 500 metres, to the west they can be absent. Within the base of the  
267 Herring Formation the Plenus Marl overlies the Hydra Formation. The Plenus Marl and the Hydra  
268 Formation are composed of relatively ductile shale and marl. They form part of the primary seal  
269 (caprock) to the Captain Sandstone in conjunction with the underlying Rodby and Carrack  
270 formations. The total thickness of these strata can be of the order of 200 metres. However, in some  
271 areas it is known that the Rodby and Carrack formations are not present. Beneath these low  
272 permeability rocks is the Captain Sandstone (a member of the Wick Sandstone Formation). The  
273 Captain Sandstone is informally subdivided into an Upper Captain Sandstone Unit, the Mid Captain  
274 Shale, and the Lower Captain Sandstone. The Lower Captain Sandstone is ubiquitous throughout the  
275 study area, the Uppermost Captain Sandstone is absent to the west of the area and over the Captain  
276 Ridge (Pinnock et al. 2003). The Captain Sandstone is usually of the order of 100 metres thick.  
277 However, in some areas the lower Captain Sandstone can be two or three times this thickness. The  
278 Captain Sandstone is laterally equivalent to the Valhall Formation which is underlain by the Humber,  
279 Fladen and Heron groups. The Humber and Heron comprise various sedimentary strata and the  
280 Fladen group comprises volcanic deposits forming the Jurassic and Triassic succession. The  
281 underlying Zechstein Group marks the top of Permian strata and an impermeable base including a  
282 number of evaporite deposits. The combined thickness of the Humber and Heron groups is of the  
283 order of several kilometres.





285 **Figure 2 Generalised stratigraphy profile of the study area, from the BGS, Johnson and Lott (1993) and Knox and**  
 286 **Holloway (1992), reproduced from SCCS (2011).**

287



288

289 **Figure 3 Geological cross-section of the Captain Sandstone Fairway. Line of cross-section shown in Figure 1. Numbered**  
 290 **profiles selected for construction of the 3D geomechanical model as marked (SCCS 2015).**

291 **Table 1 Profiles and depths of strata**

	Profile 1	Profile 2	Profile 3	Profile 4	Profile 5	Profile 6	Profile 7	Profile 8
Distance from west (m)	0.00	21000.00	33200.00	48000.00	70000.00	87600.00	96500.00	122300.00
X Coordinate (m)	0.00	20185.04	31278.53	43930.97	64675.98	83032.22	92080.20	118555.24
Y Coordinate (m)	33944.48	35860.16	25085.75	16225.53	8683.17	7937.83	7054.72	6244.38
Top of Overburden (m)	-89.91	-148.64	-106.97	-121.74	-124.46	-122.34	-132.04	-144.96
Top of Secondary Seal (m)	-854.73	-1202.99	-1230.43	-1461.32	-1705.97	-1647.65	-1743.91	-2439.41
Top of Primary Seal 2 (m)	-1212.96	-1473.68	-1435.09	-1714.25	-1902.58	-2284.43	-2375.33	-3050.18
Top of Primary Seal 1 (m)	-1265.22	-1531.37	-1498.32	-1781.02	-1960.86	-2451.34	-2495.69	-3152.39
Top of Reservoir (m)	-1321.39	-1652.41	-1597.72	-1906.36	-2008.38	-2524.80	-2556.16	-3316.58
Top of Underburden (m)	-1407.80	-1760.45	-1645.26	-2036.00	-2055.92	-2637.13	-2703.08	-3398.69
Base of Underburden (m)	-2207.80	-2560.45	-2445.26	-2836.00	-2855.92	-3437.13	-3503.08	-4198.69
Interpreted top surface (m)	-89.91	-105.44	-103.00	-103.39	-110.52	-122.34	-127.68	-144.96
Interpreted surface base (m)	-2207.80	-2712.42	-2694.33	-2759.32	-3040.37	-3437.13	-3619.82	-4198.69

292

293 For the evaluation of the storage of CO<sub>2</sub> in the subsurface it is necessary to consider the behaviour of  
 294 different strata as a response of their material characteristics in terms of the key processes  
 295 considered. To do this the profile is divided into key geo-mechanical facies comprising a passive  
 296 overburden, an active (sealing) overburden, the storage reservoir sandstone and the underburden  
 297 (Edlmann et al. 2014). The term geo-mechanical facies expresses the fact that different geological  
 298 units can be grouped together in terms of their material behaviour (fluid and mechanical behaviour)  
 299 and perceived role in an applied engineering application. The geo-mechanical facies may contain  
 300 different geological units, but as a group have a distinct role in terms of engineering application, in  
 301 this case CO<sub>2</sub> containment at depth. For the Captain Sandstone Fairway we identify five  
 302 geomechanical facies, the Reservoir, the Underburden, the Primary Seal, the Secondary Seal and the  
 303 Passive Overburden.

304 The "Reservoir" geomechanical facies is the group of generally relatively high porosity and  
 305 permeability geological units into which the CO<sub>2</sub> is being injected and where, through a variety of  
 306 processes, the CO<sub>2</sub> is to be stored (members of the Wick Sandstone Formation, Figure 2). The  
 307 "Underburden" geomechanical facies comprises those strata underlying the base of the reservoir  
 308 (Figure 2) and also the underlying lithostratigraphical units (Humber, Fladen, Heron and Zechstein

309 groups, Table 2). The Underburden is usually taken to be passive in terms of its influence on the  
 310 storage formation. However through this modelling investigation we show that the nature of the  
 311 Underburden significantly effects both the storage capacity and the sealing capacity of the system.  
 312 The active sealing overburden, or caprock, and other sealing members comprise units capable of  
 313 resisting fluid flow over thousands of years and provide mechanical restraint and sealing to the  
 314 build-up of fluid pressure in the reservoir as a result of the injection of CO<sub>2</sub>. In this case two “Primary  
 315 Seals” and a “Secondary Seal” are identified. The “Passive Overburden” comprises strata not  
 316 contributing to the fluid sealing capacity of the reservoir but providing support to the sealing layers  
 317 through its weight. For the Captain Sandstone Fairway the five geomechanical facies identified are  
 318 listed in Table 2 below.

319 Table 2 Division of strata into geomechanical facies.

Geomechanical Facies	Members
Passive Overburden,	Recent formations of the Norland Group  Cenozoic formations of the Moray Group and the Montrose Group.
Secondary Seal	Upper Cretaceous and Lower Tertiary formations of the Chalk group, that is the Ekofisk Formation, the Hod Formation, the Mackerel Formation and the Herring Formation excluding the Plenus Marl at the base.
Primary Seal 2  Primary Seal 1	Plenus Marl  Hydra Formation  Rodby Formation  Carrack Formation.
Reservoir	Comprising the Captain Sandstone and other members of the Wick Sandstone Formation.
Underburden	The Valhall Formation below the Captain Sandstone, the Humber Group, the Fladen Group and the Heron Group assumed to extend to the Zechstein Group at the top of the Permian.

320 **Tier 2: Applying an analytical geomechanical model for evaluating stability**  
 321 **under static stress conditions**

322 During injection of CO<sub>2</sub> into the reservoir, two regimes can be identified; the near-field and the far-  
 323 field. The near-field effects are caused by a sharp change in the spatial gradients of field variables of  
 324 temperature, fluid pressure, and rock stress. In the case of fluid injection there is a sharp increase in  
 325 fluid pressure in the vicinity of the injection well. Likewise in the case of a thermal effect, there is an  
 326 abrupt change in the temperature in the vicinity of the injection well. In the far field there is a  
 327 general gradual increase in fluid pressure.

328 Increasing the fluid pressure or changing the temperature of a rock can lead to the development of  
 329 new fractures or movement along a pre-existing fracture plane. This leads to a change in the  
 330 geometry of the material and a change in the medium properties of the material. Generally such  
 331 changes will accommodate fluid flow through the material as a means of reducing and relieving the  
 332 increased pressure or thermal stress placed on the material. This failure will lead to the function of  
 333 the geomechanical facies being impaired should its main role in an engineering sense be the

334 retention of fluids, stored CO<sub>2</sub> in this case. Whether a facies is stable or likely to fail depends on the  
 335 stress on the facies and some characteristic geomechanical parameters described below.

336 In our assessment of the stability of the primary and secondary seals, we took into account tensile  
 337 failure, rock fracturing and movement along a pre-existing fracture planes. Several text books deal  
 338 with the methods of calculating tensile, shear and normal stress e.g. Jaeger et al. (2007). Orientating  
 339 the axis such that the principle stresses line up with the axis x,y,z we can write for the normal stress  
 340 across the plane  $\sigma_n$  (Pa)

$$341 \quad \sigma_n = l^2 \sigma_v + m^2 \sigma_H + n^2 \sigma_h \quad (1)$$

342 where l is the directional cosine for the angle between the normal to the plane and the vertical  
 343 principal stress axis, m and n likewise for the horizontal stress axes. And for the shear stress parallel  
 344 to the plane,  $\tau$ , we can write

$$345 \quad \tau = \sqrt{(l^2 \sigma_v^2 + m^2 \sigma_H^2 + n^2 \sigma_h^2 - \sigma_n^2)} \quad (2)$$

346 The relationship between the maximum shear stress, or the shear stress which will cause failure  $\tau_f$   
 347 and the normal stress across a plane is given by

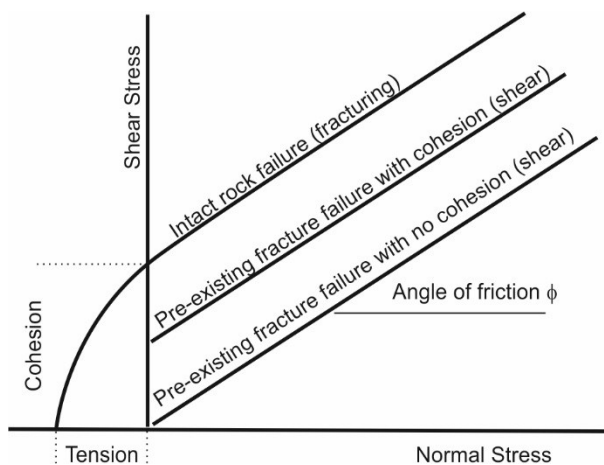
$$348 \quad \tau_f = c + (\sigma_n - \alpha u) \tan \phi \quad (3)$$

349 where  $\phi$  is the angle of friction of the failure plane,  $c$  represents the cohesive strength of the rock  
 350 or plane and  $u$  is the fluid pressure (Pa). The amount of pressure transferred from the pore or  
 351 fracture space to the skeleton can be expressed in its simplest form above with the Biot Willis  
 352 coefficient,  $\alpha$ , a ratio of fluid pressure to transferred rock pressure.

353 For intact rock, cohesion can be calculated from the standard rock parameter the Unconfined  
 354 Compressive Strength (UCS) as

$$355 \quad c = \frac{UCS(1 - \sin \phi)}{2 \cos \phi} \quad (4)$$

356  
 357



358  
 359  
 360 **Figure 4 Typical characteristics of rock failure**

361 The impact of thermal stress on the effective stress can also be evaluated such that

362

$$\sigma' = \sigma + Kr\beta E\Delta T \quad (5)$$

363 Where  $\Delta T$  ( $K^\circ$ ) is a temperature change in degrees kelvin, Kr (-) is a coefficient of restraint e.g.  
 364 (McDermott et al. 2006b; Tenzer et al. 2010),  $\beta$  is the thermal expansion coefficient ( $K^{-1}$ ) and  $E$  is  
 365 the elastic modulus of the rock. Cooling is approximately isotropic, and likewise the elastic  
 366 properties of the material in the reservoir are assumed isotropic. Heterogeneity can be seen at a  
 367 larger scale considering the layered nature of the storage system, and this will be revisited later.  
 368 Assuming full restraint in all directions the general impact of the thermal stress is to augment the  
 369 impact of the increase of fluid pressure and move the Mohr's circles further to the left, and closer to  
 370 the failure envelope. Under certain heterogeneous conditions however the superposition of the  
 371 thermal stress, and an effect known as stress bridging can be shown to increase the confining stress.

372 The likelihood of the rock failing under a given stress regime can be expressed by a factor of safety.  
 373 The factor of safety F is the ratio of disturbing forces to restraining forces. When the value is 1 or less  
 374 a breach in the strata can be assumed to have occurred.

$$F = \frac{\tau_f}{\tau} \quad (6)$$

376 In engineering terms if F is larger than 1 then there are more restraining forces than disturbing  
 377 forces. Usually during engineering design for construction a Factor of Safety of at least 1.3 is  
 378 required. For critical works a higher value may be required.

379 Where the slip plane is not already determined by the presence of a discontinuity, the safety of the  
 380 orientation most likely to fail needs to be evaluated. To do this the principal stress directions need to  
 381 be calculated taking into account the superposition of thermal stress, fluid stress and rock stress  
 382 which can lead to rotation of the principal stress axis away from the chosen coordinate system. If the  
 383 direct stresses and shear stresses in a particular coordinate system are known the orientation and  
 384 size of the principal stresses can be calculated as follows (Lewis and Schrefler 1998)

$$p = -\frac{1}{3}(\sigma_x + \sigma_y + \sigma_z) \quad (7)$$

$$q^2 = \sigma_x(\sigma_x - \sigma_y) + \sigma_y(\sigma_y - \sigma_z) + \sigma_z(\sigma_z - \sigma_x) + 3(\tau_{xy}^2 + \tau_{yz}^2 + \tau_{zx}^2) \quad (8)$$

$$\theta = \frac{1}{3} \sin^{-1} \left[ -\frac{27J_3}{2q^3} \right] \quad (9)$$

$$J_3 = \begin{vmatrix} \sigma_x + p & \tau_{xy} & \tau_{zx} \\ \tau_{xy} & \sigma_y + p & \tau_{yz} \\ \tau_{zx} & \tau_{yz} & \sigma_z + p \end{vmatrix} \quad (10)$$

389 The three principal stresses at any location are then evaluated as

$$\begin{pmatrix} \sigma_1 \\ \sigma_2 \\ \sigma_3 \end{pmatrix} = \begin{pmatrix} p \\ p \\ p \end{pmatrix} - \frac{2}{3}q \begin{pmatrix} \sin\left(\theta - \frac{2}{3}\pi\right) \\ \sin\theta \\ \sin\left(\theta + \frac{2}{3}\pi\right) \end{pmatrix} \quad (11)$$

391 Following this the factor of safety for a rock unit can be expressed as

392

$$F = \left( \frac{\frac{c}{\cos\phi} + \left( \frac{(\sigma_1 + \sigma_3)}{2} \right) \sin\phi}{\left( \frac{(\sigma_1 - \sigma_3)}{2} \right)} \right) \quad (12)$$

393

394 For the case where there is a plane of given orientation, such as a fault or a pre-existing fracture  
 395 plane, the fluid pressure likely to cause failure on this plane can be evaluated. From (1) and (2) the  
 396 normal stress  $\sigma_n$  and the shear stress  $\tau$  are known, by rearranging (3) we can show that the  
 397 minimum fluid pressure which will cause shear  $u_f$  will be

398

$$\frac{\tau - c}{\tan\phi} - \sigma_n = -u_f \quad (13)$$

399 One further constraint on fluid pressure is that it may not exceed the horizontal stress. Using the  
 400 above equation it is possible to find an orientation where the rock will not slip as it is being held  
 401 together by cohesive forces, but the fluid pressure is higher than the horizontal stress. In this case  
 402 we assume a default safety consideration that the rock does not exhibit tensile strength and that  
 403 failure will occur.

#### 404 DATA SOURCES AND PARAMETER SELECTION

405 Hydraulic, thermal and mechanical parameters were collected from a number of sources (Scottish  
 406 Power CCS Consortium 2011a,b,c, Chang et al. 2006, and references therein). Where data was not  
 407 available then typical literature values of those parameters were assigned. An overview of the  
 408 parameters is given in Table 3.

409 **Table 3 Overview of Hydraulic, Thermal and Mechanical Parameters Selected for THM Simulation of the Captain**  
 410 **Sandstone Fairway**

Formation	Geomechanical Facies	Hydraulic Parameters			Mechanical Parameters, Worst Case				Mechanical Parameters, Reasonable			
		Porosity n	Permeability k	Storage S (1/Pa)	Cohesion c (MPa)	Friction Angle $\phi^\circ$	Elastic Modulus E (GPa)	Poisson's ratio $\nu$	Cohesion c (MPa)	Friction Angle $\phi^\circ$	Elastic Modulus E (GPa)	Poisson's ratio $\nu$
Norland Coals Dornoch	Passive Overburdan	0.31	152mD	2.08E-10	10	10	3	0.46	10	10	3	0.46
Chalk Group	Secondary Seal	0.06	0.63nD	4.97E-11	0	28	30	0.32	0	28	30	0.32
Rodby Carrack Plenus Hidra	Primary Seal 1 Primary Seal 2	0.06	0.15nD	7.98E-11	0	13	10	0.38	6	13	10	0.38
Captain	Reservoir	0.2	613mD	1.30E-10	0	20	20	0.25	3	34	20	0.25
Valhall Humber Heron	Underburdan	0.09	9.25mD	7.67E-11	10	20	20	0.3	10	20	20	0.3
<b>Thermal Parameters</b>					<b>Fluid hydraulic parameters</b>							
Thermal expansion coefficient		1.10E-05			Fluid Viscosity				0.0004 Pa s			
Thermal conductivity of rock		3 W/m*K			Fluid Density				1019 kg/m <sup>3</sup>			
Heat capacity of rock		1000 J/kg*K			Average salinity				19 g/l			
*Density of formation		2550 kg/m <sup>3</sup>										
**Reservoir Longitudinal Heat Dispersivity		5 m			<b>Other contants</b>							
**Reservoir Transverse Heat Dispersivity		5 m			Biot Willis Coefficient				1			
Fluid Heat Capacity		4280 J/kg										
Fluid Heat Conductivity		0.6 W/m*K			*Calculation of initial stress state =f(depth), see text.							
Reservoir temperature		83 °C			**See text							
Sea bed temperature		5 °C										

411

412 The permeability and porosity of the geomechanical facies were derived from the static geological  
 413 model. The values provided by this report were converted into effective permeability whereby

$$414 \quad k = k_{BGS} NTG \quad (14)$$

415 Where the NTG is the Net sandstone To Gros thickness ratio, representing the volumetric ratio of  
 416 the cells open to fluid flow,  $k_{BGS}$  is the mean permeability value, and  $k$  is the effective permeability  
 417 of the cells for numerical modelling.

418

419 The compressibility  $C_m$  ( $Pa^{-1}$ ) of a rock unit is given by

$$420 \quad C_m = \frac{1(1-2\nu)(1+\nu)}{E(1-\nu)} \quad (15)$$

421 The specific storage  $Ss$  ( $Pa^{-1}$ ) is given by

$$422 \quad Ss = (C_m + nC_w) \quad (16)$$

423 The calculation of the storage parameters is given in Table 4. The compressibility of fluid (brine is  
 424 assumed as this is being forced out of the way to accommodate the CO<sub>2</sub>) is  $4.4 \times 10^{-10} Pa^{-1}$ . The  
 425 NTG ratio is not taken into account in the storage calculation as we assume the whole geological unit  
 426 will experience the stress changes due to fluid injection.

427

428 **Table 4 Calculation of specific storage parameters**

	Passive Overburden	Secondary Seal	Primary Seal	Reservoir	Underburden
n (Porosity)	0.31	0.06	0.06	0.20	0.09
v (Poisson's ratio)	0.46	0.32	0.38	0.25	0.30
E (Youngs Modulus) $Pa$	3.00E+09	3.00E+10	1.00E+10	2.00E+10	2.00E+10
Ss (Specific storage) $Pa^{-1}$	2.08E-10	4.97E-11	7.98E-11	1.30E-10	7.67E-11

429

430 Shell (2011a) report a thermal expansion coefficient of the order of  $1.1 \times 10^{-5} K^{-1}$  which is at the  
 431 higher end of what would be expected, but not unreasonable.

432 Values commonly found in the literature were assumed for the rock thermal conductivity, fluid  
 433 thermal conductivity, specific heat capacity of rock, specific heat capacity of water. Approximating  
 434 the injection of scCO<sub>2</sub> using single phase brine flow will lead to an overestimation of the impact of  
 435 the thermal pulse. The heat dispersion diffusion coefficient is taken to be approximately one half the  
 436 mesh spacing for stability reasons. The use of the heat dispersion diffusion coefficient represents  
 437 mixing and spreads the front of the heat signal out.

### 438 STRESS PROFILE AND TEMPERATURE GRADIENT

439 A hydrostatic pore pressure gradient of 10 kPa/m has been measured in the formations below the  
 440 reservoir, to a depth of circa 3000 m, Shell (2011b). This equates to an average pore fluid density of  
 441  $1019.4 kg / m^3$ . The pore fluid pressure at any depth is then given by (17), where  $z$  is depth below  
 442 surface, and  $g$  is the acceleration due to gravity =  $9.81 m / s^2$ .

$$443 \quad u = 1 \times 10^5 + 1019.4zg \quad (17)$$

444 From the Shell pore pressure prediction report (Shell 2011b) the minimum horizontal total stress is  
 445 given as

$$\begin{aligned}
 \sigma_3(\text{psi}) &= 0.421 * \text{TVDSS}(\text{ft})^{1.049} &< 6000 \text{ft} \\
 \sigma_3(\text{psi}) &= 0.0067 * \text{TVDSS}(\text{ft})^{1.5254} &> 6000 \text{ft}
 \end{aligned}
 \tag{18}$$

447 where TVDSS is True Vertical Depth Sub Sea level. These can be expressed in (m) and (MPa) as

$$\begin{aligned}
 \sigma_3(\text{MPa}) &= (0.421 * \text{TVDSS}(c_1 z(\text{metres}))^{1.049}) / c_2 &< 1828 \text{m} \\
 \sigma_3(\text{MPa}) &= (0.0067 * \text{TVDSS}(c_1 z(\text{metres}))^{1.5254}) / c_2 &> 1828 \text{m}
 \end{aligned}
 \tag{19}$$

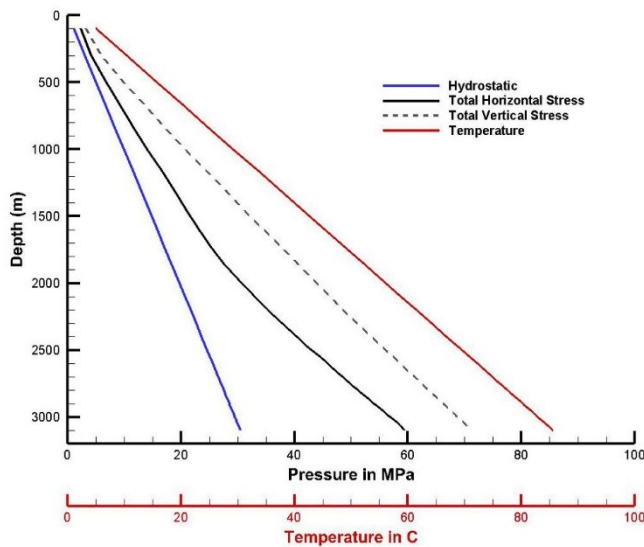
$c_1 = 3.2808399 \quad c_2 = 145.0377$

449 The shell profile for total minimum horizontal stress has been derived as far as possible from the  
 450 lower margins of the possible Leak Off Test data available.

451 The vertical total stress profile is given as

$$\sigma_v = -0.4545 + 0.0204z + 9.0043e - 7z^2
 \tag{20}$$

453 The thermal gradient was estimated for the storage complex, with the reservoir at a depth of 3000  
 454 m taken to be at a temperature of 83°C, and a sea floor temperature of 5°C. The initial conditions  
 455 summarized above are illustrated below in Figure 5



456  
 457 **Figure 5 Initial conditions assumed in the storage complex**

458 The assumptions about the mechanical failure parameters of the different geomechanical facies can  
 459 be tested using a model relating the normal stress, the shear stress and the failure parameters of the  
 460 unit to the expected in situ stress. Equation (13) provides the relationship between these  
 461 parameters, and the equations (1) and (2) describe how the normal and shear stress can be  
 462 calculated for static conditions. All possible orientations of failure planes with a resolution of 5° were  
 463 analysed to determine the lowest fluid pressure required to trigger failure under static conditions.  
 464 The in situ stresses were calculated as a function of depth using the functions described above.

465 The results of the evaluation are presented in Table 5 for the “Worst Case” (Table 3) parameters for  
 466 the Primary Seal, the “Reasonable Case” (Table 3) parameters for the Primary Seal and the “Fault  
 467 Present” for the Secondary Seal, assuming no cohesion and only an angle of friction. These are cases



468 1, 2 and 3 respectively listed in Table 5. Values where the factor of safety is less than 1 are not  
469 recorded as these are scenarios which are not physically possible.

470 The first column in Table 5 represents depth below mean sea level, the following three columns are  
471 the fluid pressure, horizontal stress and vertical stress derived from the functions given above. Three  
472 cases 1, 2, and 3 are then presented, with the rock mechanical parameters listed at the top of each  
473 case. "Rest Safety Ratio" refers to the factor of safety under natural static conditions, i.e. no  
474 injection of fluid. "Overpressure at failure" refers to the amount of fluid pressure which can be  
475 sustained in a local, static, not regional sense. This might be understood as a pulse injection, not  
476 influencing the horizontal stress field. The static analytical modelling results are compared with  
477 dynamic numerical modelling results in Tier 4: Numerical model. "FP:SH at failure ratio" indicates the  
478 ratio of the fluid pressure to the horizontal stress when the "Overpressure at failure" is applied.

479 The results indicate that the parameter set representing the "Case 1: Worst Case" is not valid under  
480 static conditions as the primary seal would not be able to withstand this stress at levels down to  
481 2600 metres under natural conditions. As this stress condition can be measured in the field, this is an  
482 indication that the mechanical parameters must be more resilient, i.e. closer to the "Case 2:  
483 Reasonable Case" parameters.

484 Examination of the Case 2 results indicates that failure with these rock mechanical parameters is due  
485 to the horizontal stress being exceeded, i.e. tensile failure where the total fluid pressure exceeds the  
486 total horizontal stress, and not fracturing or shear failure. Case 3 represents the pre-existing faults  
487 within the strata with no cohesion. It is interesting to note that the evaluation suggests that down to  
488 about 1700 metres the rest safety factor is minimal, suggesting that the stress distribution at this  
489 level is controlled by the presence of faulting. Failure within these strata can be triggered by a fairly  
490 low fluid overpressure. This depth is approximately the depth of the Passive Overburden and  
491 Secondary Seal contact. The secondary seal correlates with the stronger chalk group, and an increase  
492 in rate of positive increase in horizontal stress with depth.

493 The stability profile has been evaluated for the data on the stress profiles taken in the vicinity of the  
494 Goldeneye Gas Field (Shell, 2011a). The change in horizontal stress profile occurs at around the  
495 commencement of the Chalk Group. This is most likely due to stress bridging by the mechanically  
496 more resilient Chalk Group in the profile. It is probable that the stress profile is dependent on the  
497 depth of the Chalk Group which would suggest that where the Chalk Group exists at shallow levels,  
498 more stability can be expected due to larger horizontal stress than predicted by the evaluation  
499 presented here.

**Table 5 Fluid pressure and safety limit for three different mechanical failure criteria.**

Depth m	Fluid Pressure MPa	Horizontal Stress MPa	Vertical Stress MPa	Case 1 C=0 MPa $\phi=13^\circ$			Case 2 C=6 MPa $\phi=13^\circ$			Case 3 C=0 MPa $\phi=28^\circ$		
				Rest Safety Ratio	Overpressure at Failure MPa	FP:SH at Failure Ratio	Rest Safety Ratio	Overpressure at Failure MPa	FP:SH at Failure Ratio	Rest Safety Ratio	Overpressure at Failure MPa	FP:SH at Failure Ratio
1000	10.1	14.16	20.85				1.40	4.06	1.00	1.03	0.29	0.73
1200	12.1	17.14	25.32				1.42	5.04	1.00	1.04	0.43	0.73
1400	14.1	20.15	29.87				1.43	6.05	1.00	1.04	0.57	0.73
1600	16.1	23.18	34.49				1.44	7.08	1.00	1.04	0.70	0.72
1800	18.1	26.23	39.18				1.45	8.13	1.00	1.05	0.82	0.72
2000	20.1	30.70	43.95				1.53	10.59	1.00	1.16	3.12	0.76
2200	22.1	35.50	48.78				1.61	13.40	1.00	1.27	5.90	0.79
2400	24.1	40.54	53.69				1.68	16.44	1.00	1.37	9.01	0.82
2600	26.1	45.80	58.67				1.75	19.70	1.00	1.48	12.44	0.84
2800	28.1	51.28	63.72	1.06	1.79	0.58	1.83	23.18	1.00	1.58	16.16	0.86
3000	30.1	56.97	68.85	1.21	6.45	0.64	1.89	26.87	1.00	1.67	20.17	0.88
3200	32.1	62.87	74.05	1.36	11.55	0.69	1.96	30.77	1.00	1.76	24.46	0.90
3400	34.1	68.96	79.31	1.50	17.05	0.74	2.02	34.86	1.00	1.85	29.02	0.92
3600	36.1	75.24	84.66	1.64	22.95	0.78	2.08	39.14	1.00	1.94	33.83	0.93
3800	38.1	81.71	90.07	1.77	29.24	0.82	2.14	43.61	1.00	2.02	38.89	0.94
4000	40.1	88.36	95.55	1.90	35.89	0.86	2.20	48.26	1.00	2.10	44.20	0.95
4200	42.1	95.19	101.11	2.02	42.91	0.89	2.26	53.09	1.00	2.18	49.75	0.96
4400	44.1	102.19	106.74	2.14	50.26	0.92	2.32	58.09	1.00	2.26	55.52	0.97

**Explanation of terms**

- Depth Depth in metres below mean sea level at which the stability is analysed
- Fluid Pressure Natural fluid pressure at depth given
- Horizontal Stress Horizontal stress at given depth
- Vertical Stress Vertical stress at given depth
- Rest Safety Ratio Factor of safety equation (6) with no fluid injection at this depth for these mechanical parameters
- Overpressure at Failure Amount of extra fluid pressure at this depth likely to cause failure
- FP:SH at Failure Ratio Total fluid pressure to horizontal stress ratio at this depth at failure. A value of 1 indicates tensile failure

1 **Tier 3: An empirical function to summarise the static geomechanical results**

2 To enable the geomechanical results to be portable to other codes and usable for the whole of the  
 3 Captain Sandstone Fairway, empirical multivariate functions were derived which allowed the  
 4 maximum possible overpressure to be retained by the Primary Seal, the Secondary Seal or Faults to  
 5 be expressed as a function of depth. It should be noted that this is for the static geomechanical  
 6 conditions, that is dynamic regional changes to the horizontal stress as a result of fluid pressure  
 7 increase is not taken into account. These are accounted for in Tier 4.

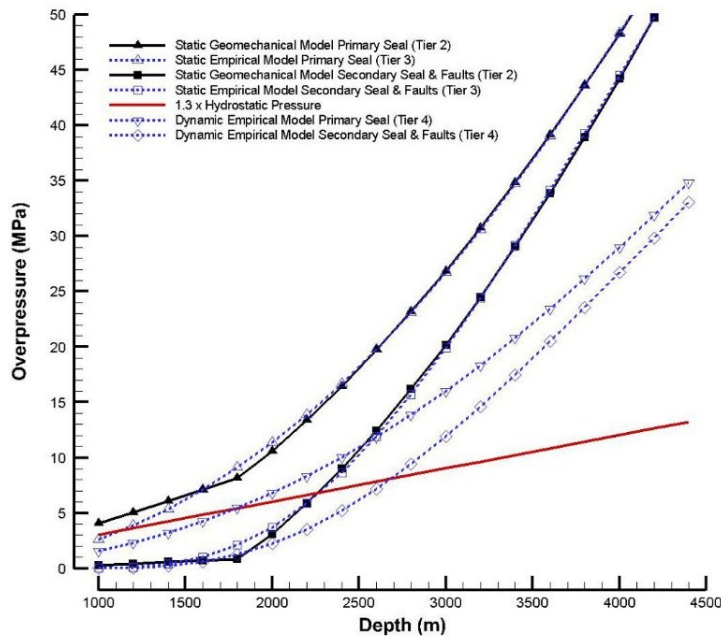
8 For the Primary Seal the maximum overpressure is given by (21) valid from 1000 metres to 4500  
 9 metres depth.

$$P_{f\_static} = \frac{a}{\left[1 + \left(\frac{z}{b}\right)^c\right]^d} \quad \begin{array}{l} a = 100 \\ b = 5601.22 \\ c = -8.17113 \\ d = 0.258517 \\ z = \text{depth in (m)} \\ P_f = \text{failure overpressure in MPa} \end{array} \quad (21)$$

11 For the Secondary Seal and Faults the maximum overpressure is given by (22), valid from 1000  
 12 meters to 4500 metres depth.

$$P_{f\_static} = e^{\left(\frac{a+b}{z}\right) + (c \ln z)} \quad \begin{array}{l} a = 9.77318 \\ b = -11011.5 \\ c = -0.3883 \\ z = \text{depth in (m)} \\ P_f = \text{failure overpressure in MPa} \end{array} \quad (22)$$

14 The modelling results presented in Table 5 are illustrated for the primary seal and the secondary seal  
 15 in Figure 6, as is the fitting using the empirical formulas given above. This figure also includes the  
 16 results of the Tier 4 modelling where the dynamic effect of regional fluid pressure increase is taken  
 17 into account.



18

19 **Figure 6 Primary Seal, Secondary Seal and Fault Overpressure Limits: Comparison of static stress (Tier 2), empirical fitting**  
 20 **(Tier 3) and dynamic stress (Tier 4) results as well as a simple hydrostatic pressure stress limit assumption.**

21 **Tier 4: Numerical modelling of dynamic stress conditions**

22 Numerical models are able to take into account heterogeneity in the analysis of the problem to be  
 23 solved. Although several simplifications have to be made, the numerical models come closer to  
 24 reality than analytical approaches. The numerical analysis performed involved the solution of the  
 25 Thermal, Hydraulic and Mechanical balance equations. The open source coupled process simulator  
 26 OpenGeoSys (OGS) was used to solve the coupled process problems. The theory and several  
 27 benchmarks regarding the use of OGS may be found in Kolditz et al. (2012). The following provides  
 28 an overview of the multi-physics problems solved.

29 Following Lewis and Schrefler (1998) the momentum balance equation can be written as

30 
$$L^T \boldsymbol{\sigma} + \rho \mathbf{g} = 0 \tag{23}$$

31 For a single solid phase,  $\rho$  is the solid density ( $\text{kg/m}^3$ ),  $\mathbf{g}$  is the acceleration due to gravity ( $\text{m/s}^2$ ).

32 The differential operator  $L$  is defined as

33

$$L = \begin{bmatrix} \frac{\partial}{\partial x} & 0 & 0 \\ 0 & \frac{\partial}{\partial y} & 0 \\ 0 & 0 & \frac{\partial}{\partial z} \\ \frac{\partial}{\partial y} & \frac{\partial}{\partial x} & 0 \\ 0 & \frac{\partial}{\partial z} & \frac{\partial}{\partial y} \\ \frac{\partial}{\partial z} & 0 & \frac{\partial}{\partial x} \end{bmatrix} \quad (24)$$

34 The stress tensor represented as a vector such that

35

$$\boldsymbol{\sigma} = \{ \sigma_x \quad \sigma_y \quad \sigma_z \quad \tau_{xy} \quad \tau_{yz} \quad \tau_{xz} \}^T \quad (25)$$

36 The strain is given as

37

$$\boldsymbol{\varepsilon} = \{ \varepsilon_x \quad \varepsilon_y \quad \varepsilon_z \quad \gamma_{xy} \quad \gamma_{yz} \quad \gamma_{xz} \}^T \quad (26)$$

38 The constitutive relationship of strain to stress is given as

39

$$d\boldsymbol{\sigma} = \mathbf{D}d\boldsymbol{\varepsilon} \quad (27)$$

40 Strain is related to displacement  $\mathbf{u}$

41

$$d\boldsymbol{\varepsilon} = Ld\mathbf{u} \quad (28)$$

42

43 This is solved as a boundary value problem where  $\mathbf{u} = \mathbf{u}_0$  in  $\Omega$  and on  $\Gamma$   $\mathbf{I}^T \boldsymbol{\sigma} = \mathbf{t}$

44 Where  $\mathbf{I}$  is related to the unit normal vector  $\mathbf{n} = \{ n_x \quad n_y \quad n_z \}^T$  by

45

$$\mathbf{I} = \begin{bmatrix} n_x & 0 & 0 \\ 0 & n_y & 0 \\ 0 & 0 & n_z \\ n_y & n_x & 0 \\ 0 & n_z & n_y \\ n_z & 0 & n_x \end{bmatrix} \quad (29)$$

46 For evaluation of coupled flow in a saturated porous medium we require the mass balance equation  
47 for fluid flow

48

$$Ss \frac{\partial p_w}{\partial t} + \text{div} \left[ \frac{k}{\mu^w} (-\text{grad } p_w + \rho_w \mathbf{g}) \right] = 0 \quad (30)$$

49 Where  $Ss$  is the specific storage of the porous media, described above in (16),  $k$  is the permeability  
50 in ( $m^2$ ),  $\mu^w$  is the viscosity of the fluid in ( $\text{Pa}\cdot\text{s}^{-1}$ ),  $p_w$  is the fluid pressure in (Pa). Coupling of the

51 fluid flow and momentum balance equations is accomplished by considering effective stress such  
 52 that

$$53 \quad \boldsymbol{\sigma}' = \boldsymbol{\sigma} - \alpha_b \mathbf{m} p_w \quad (31)$$

54 Where  $\alpha_b$  is the Biot Willis coefficient,  $\boldsymbol{\sigma}'$  is now considered to be the effective stress and

$$55 \quad \mathbf{m} = [1 \quad 1 \quad 1 \quad 0 \quad 0 \quad 0]^T \quad (32)$$

56 Strictly speaking the Biot Willis coefficient should also be evaluated in the calculation of the storage  
 57 coefficient. As a first approximation during modeling this coefficient was set at 1, meaning there is a  
 58 full transfer of fluid pressure to the rock skeletal stress, thereby making the formulation used for the  
 59 specific storage in (16) valid.

60 The solution of (30) provides the fluid pressure distribution throughout the modelled area. This can  
 61 be used to derive the fluid velocity  $\mathcal{V}$  which can then be used to solve the advective heat transport  
 62 equation given in (33)

$$63 \quad c\rho \frac{\partial T}{\partial t} + c^w \rho^w \mathcal{V} \cdot \nabla T - D \nabla^2 T = \rho Q_r \quad (33)$$

64 where  $c$  is the specific heat capacity of the saturated porous rock (J/kg.K),  $c^w$  is the specific heat  
 65 capacity of the fluid,  $D$  is the heat diffusion dispersion tensor for the porous medium,  $T$  is  
 66 temperature,  $\rho^w$  is fluid density,  $\rho$  is density of the saturated porous rock, and  $Q_r$  is the heat  
 67 source or sink. Here, after De Marsily (1986), the heat diffusion dispersion tensor contains a  
 68 component for pure diffusion and a component for dispersion due to advection, i.e.:

$$69 \quad D_\alpha = \lambda_m + v_\alpha \beta_\alpha \quad (34)$$

70 where  $D_\alpha$  is the heat diffusion dispersion coefficient in the  $\alpha$  -direction (J/Kms),  $\lambda_m$  is the  
 71 isotropic heat conductivity of the porous medium (J/Kms),  $v_\alpha$  is advective flow velocity in the  $\alpha$  -  
 72 direction, and  $\beta_\alpha$  is the heat dispersion coefficient in the  $\alpha$  -direction. The value  $\beta_\alpha$  is the product  
 73 of the directional (longitudinal or transverse) dispersion coefficient, with  $c^w \rho^w$ .

74 The inclusion of thermal stress in the evaluation is such that

$$75 \quad \Delta \varepsilon = D (\Delta \varepsilon^e - \alpha_t \Delta T) \quad (35)$$

76 where  $\alpha_t$  is the thermal expansion coefficient. A staggered finite element solution procedure was  
 77 applied to evaluate the above equations, with the order Hydraulics, Thermal, Mechanical. A more  
 78 detailed description of the finite element method can be found in works such as Lewis and Schrefler  
 79 (1998) and Zienkiewicz and Taylor (2005).

## 80 Models and Meshes

81 The aim of the modelling was to investigate in as much detail as possible the THM geomechanical  
 82 response of the Captain Sandstone Fairway during injection of dense phase CO<sub>2</sub> at multiple sites. The  
 83 results of the THM modelling were then used to augment the Tier 3 empirical model, and account  
 84 for dynamic stress. Computationally it was not possible to model the whole of the ~1300 km<sup>2</sup> area at  
 85 high resolution. Therefore models were constructed in 2D and 3D to enable key engineering relevant  
 86 parameters to be determined and the impact of coupled processes to be investigated at sufficient

87 resolution. These models, with their main features and purposes are listed in Table 6, and described  
 88 in more detail below.

89 To model the thermal pulse and the development of thermal stress in the vicinity of the injection  
 90 well, a mesh resolution significantly lower than the thickness of the geomechanical facies layers  
 91 affected was necessary. 2D cross sections using both quad and triangular elements with a mesh  
 92 resolution of ten metres in the reservoir and base of the primary seal were generated (Figure 7,  
 93 Figure 8 and Figure 9). The section dimensions were of the order of up to 3 km depth X 6 km width.  
 94 The geometry of the sections was asymmetrical hence an axisymmetric simulation was not possible.

95 To investigate the approximate magnitude of the expected fluid pressure increase in the storage  
 96 complex for the given injection rates, a 3D regional geomechanical model of the Captain Sandstone  
 97 Fairway was created with mesh dimensions of the order of 130 km length, 10 km width and 4 km  
 98 depth using non regular hexahedral elements. The mesh resolution was selected to be 50 metres in  
 99 the vicinity of the injection wells at Site A and Site B (Figure 10).

100 **Table 6 List of models and meshes, main features and purposes**

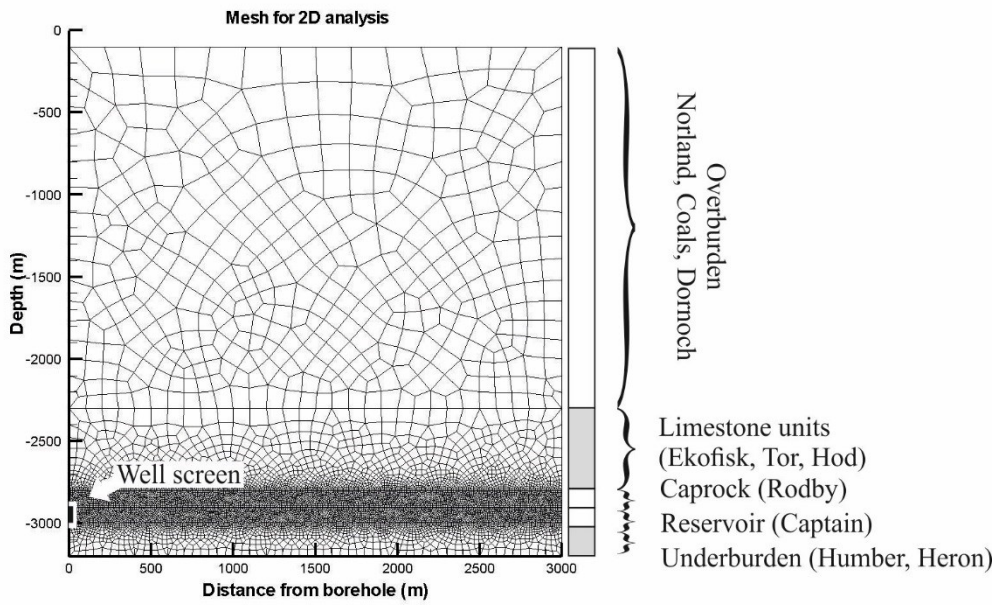
Model and key feature	Main purpose
3D Regional model 130 km x 10 km x 4 km, non-regular hexahedral elements, mesh resolution was selected to be 50 metres in the vicinity of the injection wells	Determine the magnitude of the fluid pressure increases in the reservoir expected as a result of the injection rates. Source terms in the 2D models (following) were set accordingly to generate the same fluid pressure
2D Generic cross section, where the reservoir is at a depth of 3000 m, mesh resolution down to 10 m.	Investigation of the impact of the coupling and main controls of the THM processes on fluid pressure, stress and thermal stress distribution in the storage complex.
2D Cross section at injection site A, mesh resolution down to 10 m.	Evaluation of the THM geomechanical stability in detail at site A
2D Cross section at injection site B, mesh resolution down to 10 m	Evaluation of the THM geomechanical stability in detail at site B

101

102 Due to the size of the meshes generated a number of calculations were performed using the parallel  
 103 capability of OpenGeoSys on eight cores.

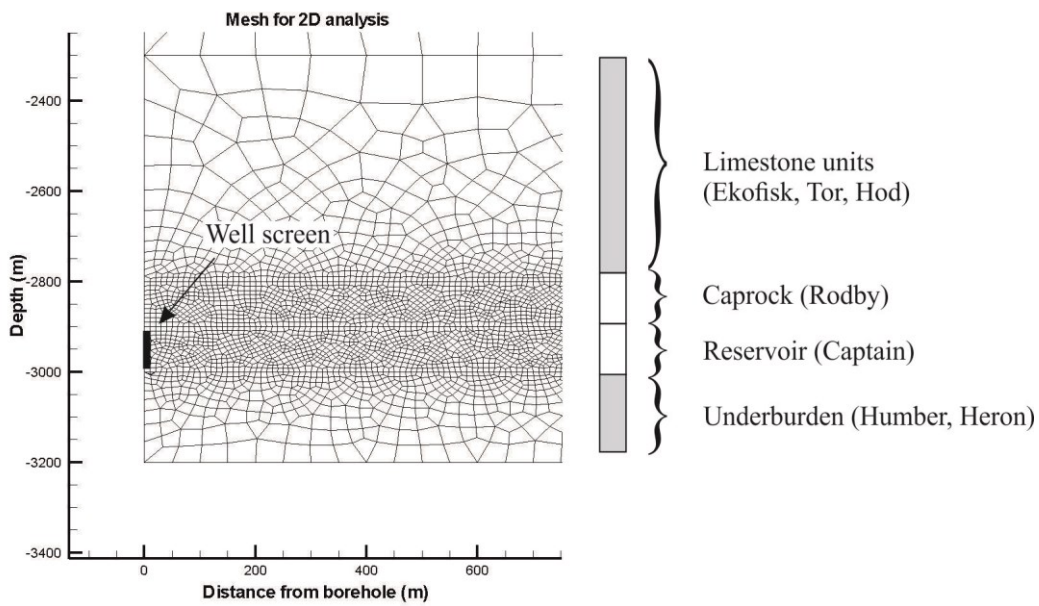
104 The meshes were generated using Gmsh, (Geuzaine and Remacle 2009), geometry selected from  
 105 data provided derived in this study and from Shell (2011a,b,c). The injection pressures predicted in  
 106 the 3D geological model at the locations of Site A and Site B were used to inform the rate of injection  
 107 in the 2D sections to match the anticipated overpressures. The injection rates in the 2D models were  
 108 chosen such that the maximum pressure predicted in the 3D models was slightly exceeded to allow a  
 109 further degree of safety.

110



111

112 Figure 7 Mesh used for 2D analysis of a general cross section for the Captain Sandstone Fairway

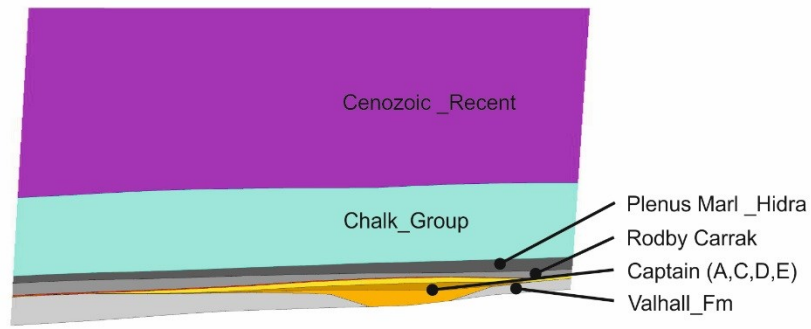


113

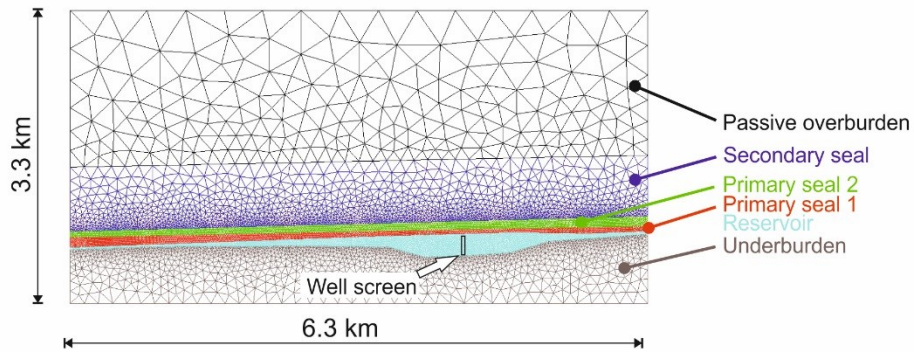
114 Figure 8 Close up view of mesh used for 2D analysis of a general cross sections for the Captain Sandstone fairway

115





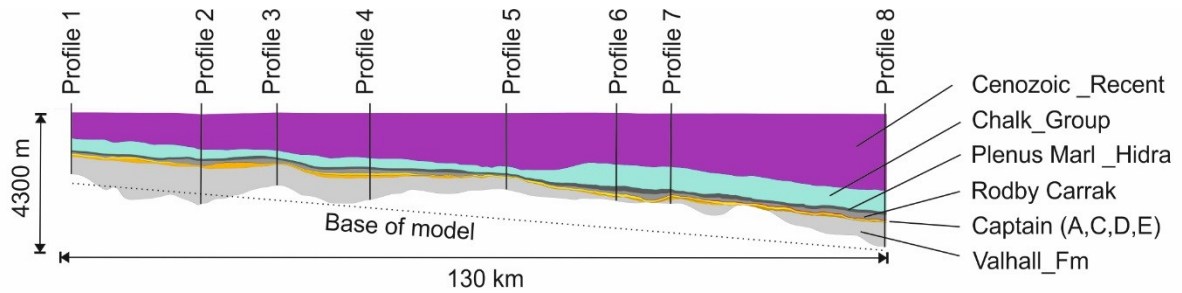
Geomechanical mesh cross section at site A



116

117 **Figure 9 Cross section of Captain Sandstone Fairway at injection site A, mesh and geometry for detailed THM modelling**

118



119

120 **Figure 10 3D mesh of the Captain Sandstone Fairway used for the evaluation of the fluid pressure response during**  
 121 **injection of dense phase CO<sub>2</sub>.**

122 **Numerical Model Validation**

123 Both the fluid pressure predictions and the deformation predictions of the numerical model were  
 124 validated against other modelling approaches and previous work.

125 Parallel to the development of the geomechanical model presented here, Eclipse was used to  
 126 simulate a discrete multiphase model of the Captain Sandstone Fairway for a single statistical  
 127 realisation of the Captain Sandstone Fairway. This model assumed that base of the reservoir facies  
 128 was closed to fluid flow. The pressure connectivity predicted between sites A and B was shown to be  
 129 very similar to the connectivity predicted by the geomechanical model with similar boundary  
 130 conditions.

131 Shell (2011a) present a 3D model of the Goldeneye Gas field whereby they investigate the surface  
 132 deformation as a result of gas extraction from the Goldeneye field. They present modelling results  
 133 for a reservoir under pressure of circa 10 MPa. They obtain a surface deformation of 4.6 cm  
 134 subsidence of the sea floor, with the deformation extending 14 km east-to-west and 9 km north-to-  
 135 south. Using the current model for the Captain Sandstone Fairway (3D model and different  
 136 geometry), with the parameterisation presented in Table 3 (injection parameters rather than  
 137 extraction parameters) the sea floor subsidence predicted by this model is 3 cm for the sea floor and  
 138 the extent is similar to the Shell (2011a) model. There is no specification of the limit of deformation,  
 139 e.g. 1 mm or less, so only an estimate of the extent can be made here.

140 Additionally the OpenGeoSys code is extensively documented with respect to comparison against  
 141 benchmarks (Kolditz and Shao 2012). Therefore it can be taken that the model is reasonably well  
 142 validated.

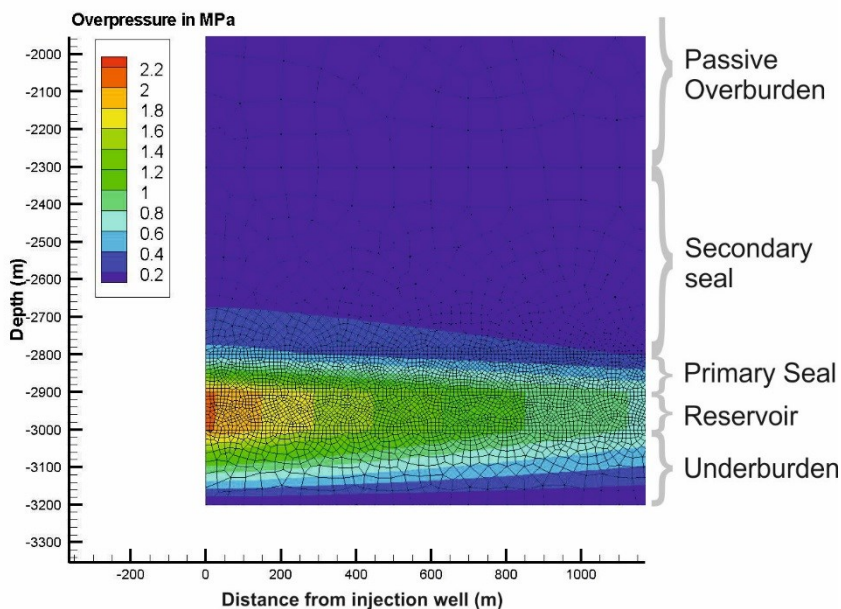
144 **Reservoir overpressure limit and impact of thermal stress**

145 Both 2D and 3D geomechanical modelling results are presented. First selected results are presented  
 146 for a generic 2D cross section in the Captain Sandstone Fairway, where the Reservoir is found at a  
 147 depth of circa 3000 metres.

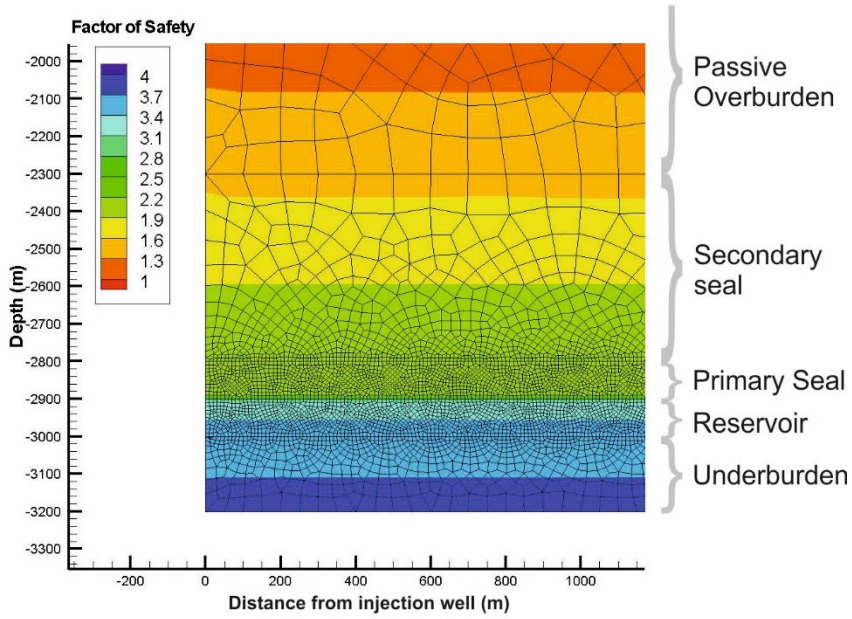
- 148 1. A fluid overpressure of 2.2 MPa at the injection well, after 30 years of injection at realistic commercial  
 149 injection rates in a generic cross section (Figure 11).
- 150 2. A fluid overpressure of 2.2 MPa and a temperature of 20°C, that is about 60°C below the reservoir  
 151 temperature, after 30 years of injection at a realistic commercial injection rate in a generic cross section  
 152 close to Site A.

153 The factor of safety prior to any injection in the vicinity of the well is presented in Figure 12. The  
 154 effect of considering only the fluid pressure in the calculation of the factor of safety for 2.2 MPa  
 155 injection overpressure is presented in Figure 13. The thermal impact of the injection of scCO<sub>2</sub> after  
 156 30 years is presented in Figure 14, and the case where both the fluid pressure and the thermal stress  
 157 is considered is presented in Figure 15.

158 To understand the impact of including the thermal stress, the change in the factor of safety from the  
 159 fluid only case to the fluid and thermal case is presented in Figure 16. The change in the factor of  
 160 safety can be directly related to the change in the horizontal stress field (Figure 17). As the Reservoir  
 161 contracts due to the thermal stress, the horizontal stress component is carried by stress-bridging  
 162 through the stiffer layers of the Chalk Group and the Underburden. The factor of safety of the Chalk  
 163 Group acting as the secondary seal increases slightly as a result of this effect. The Primary Seal,  
 164 because it is not so stiff accommodated the change in stress through more strain. Additionally the  
 165 stress field itself is rotated, Figure 18.

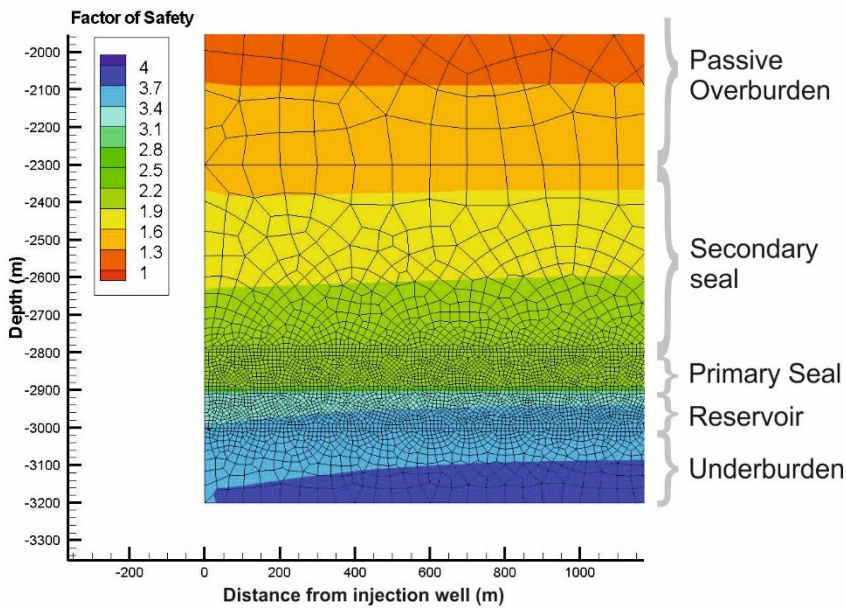


166  
 167 **Figure 11 Fluid overpressure in MPa after 30 years of injection in the 2D general model scenario, well screen bottom left,**  
 168 **~2900 m to 3000 m.**



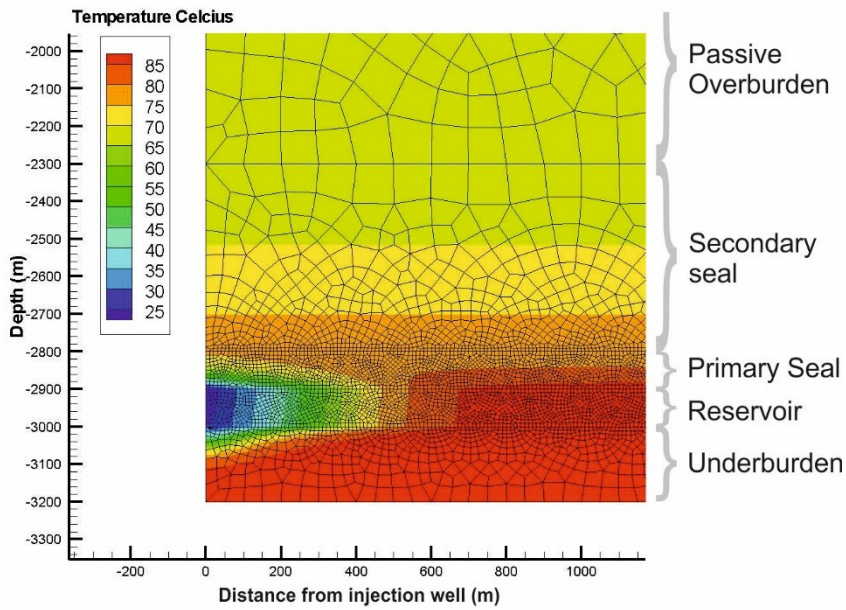
169

170 **Figure 12 Initial factor of safety without fluid injection**



171

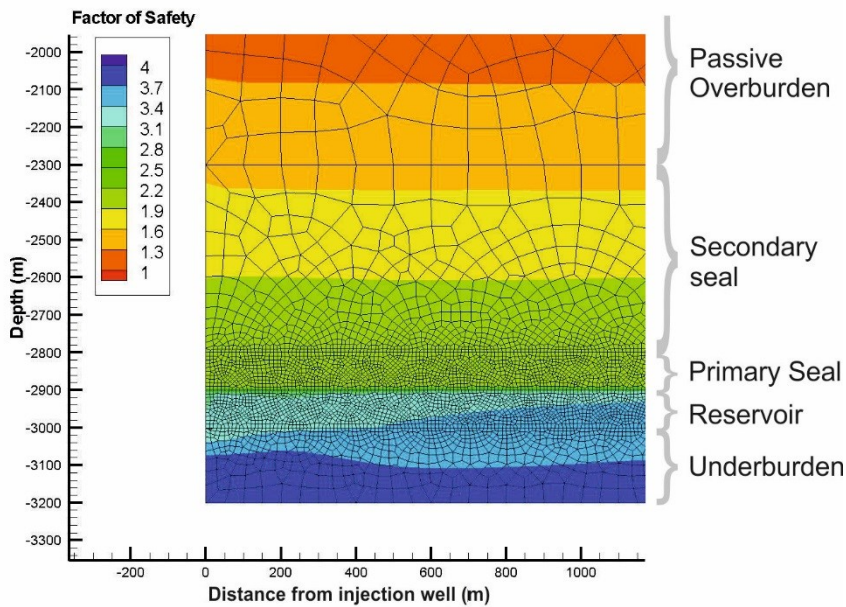
172 **Figure 13 Factor of safety for 2.2 MPa overpressure, for fluid injection without thermal stress, well screen bottom left,**  
 173 **~2900 m to 3000 m.**



174

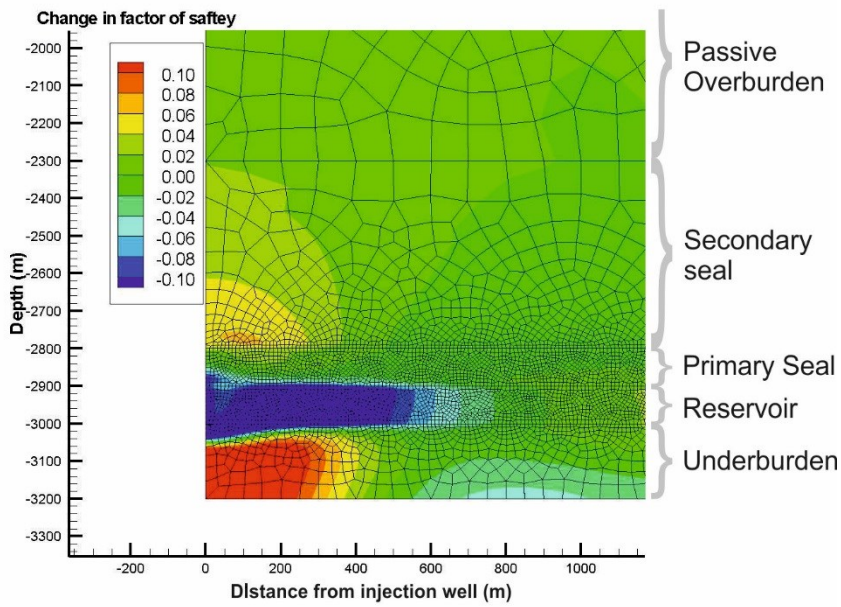
175 **Figure 14 Temperature profile after 30 years of injection in the 2D general model scenario, well screen bottom left,**  
 176 **~2900 m to 3000 m (SCCS 2015).**

177



178

179 **Figure 15 Factor of safety for 2.2 MPa overpressure, for fluid injection with thermal stress, well screen bottom left,**  
 180 **~2900 m to 3000 m.**

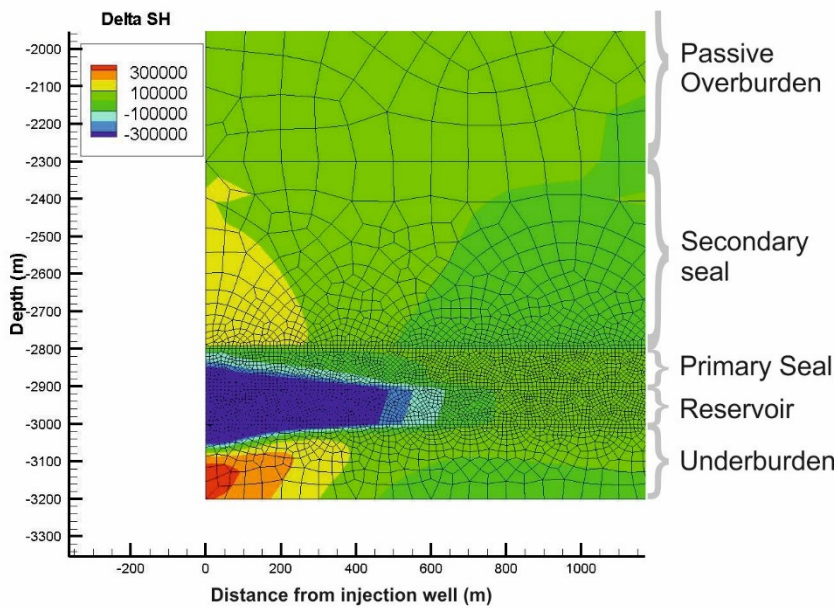


181

182

183

Figure 16 Change in factor of safety as a result of thermal stress. Positive values (pale green to red) indicate an increase in the safety factor, well screen bottom left, ~2900 m to 3000 m.

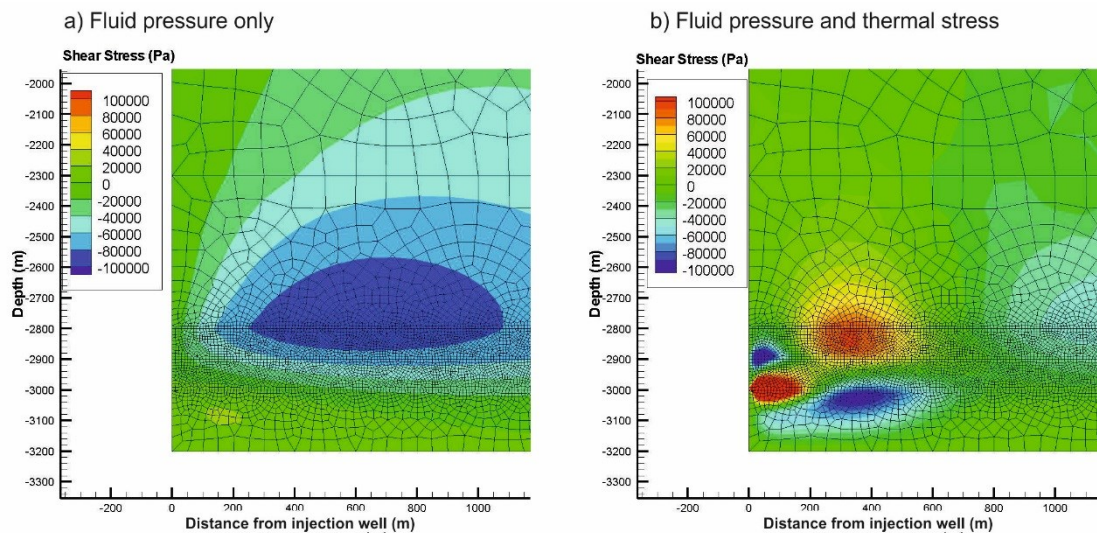


184

185

186

Figure 17 Change in horizontal stress field due to the impact of thermal stress, well screen bottom left, ~2900 m to 3000 m.



187  
 188 **Figure 18** Rotation of stress field a) caused solely by fluid injection and b) caused by fluid injection thermal stress, well  
 189 screen bottom left, ~2900 m to 3000 m (SCCS 2015).

190 The above figures (Figure 12 to Figure 18) illustrate the generic response of the Reservoir to the  
 191 injection of scCO<sub>2</sub>. The stress redistribution is a function of the nature of the interaction of the  
 192 geomechanical facies, their mechanical properties and their hydraulic properties.

193  
 194 Different strata exhibit several different orders of magnitude difference in terms of their  
 195 permeability. The location of the fluid pressure changes are controlled by the heterogeneity  
 196 between the layers in their permeability. The main fluid pressure change is seen in the reservoir  
 197 facies, and contained in the reservoir by the overlying and underlying strata.

198  
 199 In contrast the mechanical properties of the different strata are within an order of magnitude of one  
 200 another, and so the stress distribution is more wide spread. Stiffer layers carry more of the stress  
 201 loading than the softer layers and so are more effected than the softer layers by any increases or  
 202 decreases in the stress field. Hence the stress distribution follows the general trend of the strata in  
 203 terms of geometry, but this is not so pronounced as the fluid flow.

204  
 205 It can be seen from the equation (33) that the thermal pulse is controlled by a diffusive and  
 206 advective term. The diffusive thermal parameters are all of a similar magnitude. This means that the  
 207 diffusive thermal signal is spherical. However the advective thermal signal is controlled by fluid flow  
 208 and therefore directly related to the permeability distribution of the system.

209  
 210 The overprint of the thermal stress changes and the fluid stress changes on the regional stress leads  
 211 to a slight enhancement of the stability of the secondary seal. The reason for this is illustrated in  
 212 Figure 17. As the area around the injection well within the reservoir cools, so the reservoir contracts  
 213 and carries less of the regional horizontal stress meaning that the stronger overlying and underlying  
 214 strata carry more stress. These results are specific to this sequence of strata and the contrast in  
 215 mechanical and hydraulic parameters of the modelled layers.

216  
 217 Fjaer et al. 2008 showed that for a rigidly constrained plate in the horizontal plane that the longer  
 218 term change in horizontal stress due to thermal stress changes around the borehole is given by the  
 219 analytical expression

220

$$\Delta S_h = \frac{E}{(1-\nu)} \alpha_i \Delta T \quad (36)$$

221 This is an analytical model assuming fully ridged boundary conditions allowing. In this unrealistic  
 222 case it would suggest a value of up to 9 MPa change in horizontal stress for the reservoir strata and  
 223 circa 5 MPa for the primary seal for a 60 C drop in temperature. In reality the strata is not restrained  
 224 horizontally or vertically, so the strain from the thermal stress is accommodated over a large area.  
 225 The numerical model suggests that the maximum change in horizontal stress due to the thermal  
 226 stress is of the order of 0.3 MPa. The numerical model has not taken into account possible very near  
 227 borehole effects, cementing features and potential very local stress bridging. However the thermal  
 228 stress superimposes on the regional horizontal stress, which is of the order of 30 MPa. Any impact of  
 229 thermal stress within the strata of the Captain Sandstone Fairway is most likely to be localized,  
 230 minimal and of a consolidation nature.

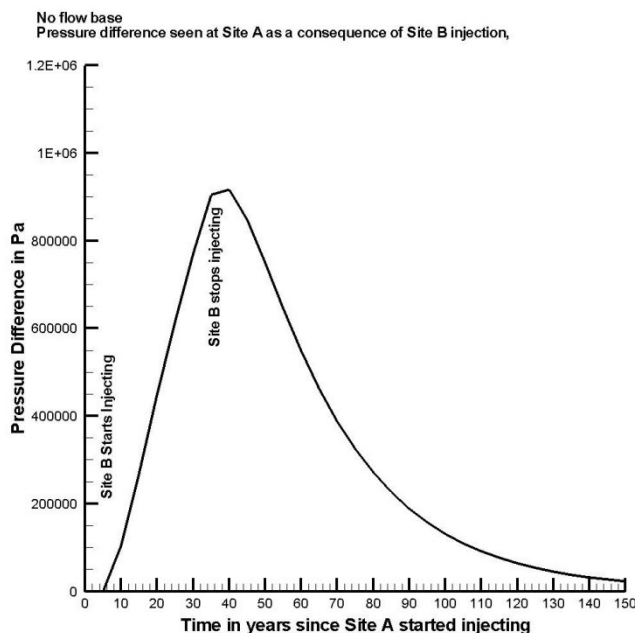
231

232 **Significance of the basal boundary (connectivity and surface deformation)**

233 During hydrocarbon production the nature of the basal boundary is usually of secondary importance.  
 234 However, when considering the regional pressure increase during fluid injection into a reservoir, the  
 235 nature of the underburden becomes highly significant. Fluid pressure in the reservoir can be  
 236 dissipated either through lateral connection to other strata, or vertically. The areal extent of the  
 237 connection of the underburden with the reservoir is extremely large, therefore even a low  
 238 permeability Underburden enables significant fluid flow and therefore makes pressure dissipation  
 239 through the Underburden very significant. The pressure connectivity between Site A and Site B is  
 240 negligible for the case where the basal boundary is open to flow but the Underburden has a  
 241 thickness of circa 800 metres.

242 For the case where the basal boundary is not open to flow the pressure connection is significant,  
 243 leading to a clear connectivity between the sites. Figure 19 demonstrates this, Site A and Site B can  
 244 be shown to have of 0.9 MPa pressure influence on each other after 15 years of injection.

245



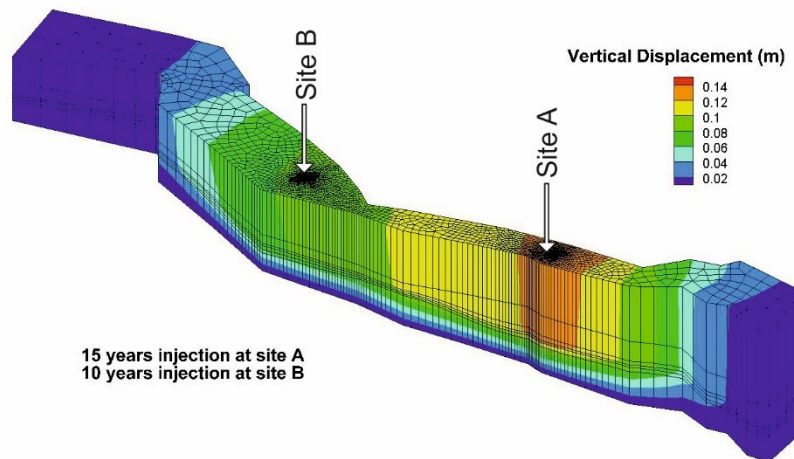
246

247 **Figure 19 Pressure connection between Site A and Site B, where model basal boundary is closed to flow. Pressure**  
 248 **difference in Pa.**

249 Where the basal flow boundary is considered closed to flow, the fluid pressure in the reservoir is  
 250 greater, and the largest amount of surface deformation is predicted, Figure 20. It is highly significant



251 that the vertical displacement in the positive direction extends below the level of the reservoir. This  
 252 means that the strata within the Underburden are hydraulically connected to the reservoir and that  
 253 the Underburden pore space is being used to accommodate fluid migration and increased pressure  
 254 in the reservoir.



255  
 256 **Figure 20 Deformation after 15 years CO<sub>2</sub> injection at Site A and 10 years injection at Site B, at an annual rate of 6**  
 257 **Mt/year at both sites with free surface boundary and a no-flow boundary at the base of the model**

258  
 259 **Combination of the static and dynamic geomechanical THM modelling results**  
 260 **to provide a location dependent look up function.**

261 In this section Tier (3) results are combined with the Tier (4) modelling to provide the final look up  
 262 function to evaluate the maximum fluid pressure possible in various strata of the storage system.

263 The Tier (3) empirical function is based on the fitting of the analytical evaluation of the static stress  
 264 conditions. Under static equilibrium conditions of stress, the vertical stress can be shown to be  
 265 directly related to the horizontal stress in the strata, assuming no further tectonic stresses, where  $\nu$   
 266 is Poisson's ratio:

267 
$$\sigma_H = \sigma_h = \frac{\nu}{1-\nu} \sigma_v \tag{37}$$

268 When the fluid pressure in the reservoir is increased both the vertical stress and the horizontal  
 269 stress is affected. Hillis (2001) and Kim and Hosseini (2014) show that the change in horizontal stress  
 270 as a result of fluid injection into a reservoir can be evaluated to

271 
$$\Delta\sigma_H = \Delta\sigma_h = \Delta P\alpha \frac{1-2\nu}{1-\nu} \tag{38}$$

272 where  $\alpha$  is the Biot Willis coefficient. The change in vertical stress (Kim and Hosseini 2014) can be  
 273 shown to be

274 
$$\Delta\sigma_v = \Delta P \frac{\alpha}{2} \frac{1-2\nu}{1-\nu} \quad (39)$$

275 Under static conditions the initial fluid pressure change would be under the stress conditions  
 276 expressed in (37), under prolonged conditions of fluid pressure increase, where there is a regional  
 277 fluid pressure change then (38) and (39) describe the dynamic stress conditions and the horizontal  
 278 and vertical stress change respectively.

279 The relationship between the dynamic stress conditions and static stress conditions is therefore  
 280 consistent throughout the storage complex, allowing a consistent relationship to be developed  
 281 between the dynamic stress conditions and the static stress conditions.

282 For typical values of the Poisson’s ratio the value of  $\frac{1-2\nu}{1-\nu}$  is usually between 0.5 and 0.6. This  
 283 means that for a regional fluid pressure increase there will be a partial reduction in the horizontal  
 284 stress and less noticeable reduction in the vertical stress. Both of these changes impact consistently  
 285 throughout the profile on the evaluation of the stability of the geomechanical facies and faults in the  
 286 storage system. However this does not directly lead to a 0.5 to 0.6 reduction in the maximum  
 287 predicted safe overpressure of the strata for the following reasons

- 288 • The change in fluid pressure is superimposed on the already present stress field, the change in fluid pressure  
 289 may be of the order of 1-10 MPa, the existing horizontal stresses are already of the order of 20 – 40 MPa
- 290 • The analytical model assumes perfect isotropic homogeneous conditions under static stress loading. The  
 291 numerical THM model accounts for the dynamic stress conditions, for the heterogeneity in the geological  
 292 strata, for geometrical differences in the layers and for the impact of the thermal stress.

293 The Tier 4 THM modelling is used to predict the maximum overpressure the reservoir can sustain.  
 294 These predications are then compared to the Tier 3 empirical predictions. Table 7 present the fluid  
 295 pressure results and safety factors from the 3D and 2D models at sites A and B. The 3D model  
 296 provided the predicted overpressure in the reservoir as a function of the expected injection rates in  
 297 the storage asset (5.8 MPa, 6.0 MPa). These overpressures were then simulated with slight safety  
 298 margin in the 2D sections (6.3 MPa, 6.6 MPa). The ratio of horizontal stress to fluid pressure and the  
 299 minimum factors of safety to shear failure were then determined in the profile. In some cases the  
 300 worst case values were clearly impacted by the local geometry of the layers and a small distance  
 301 from the injection wells. It can be seen that at 6.6 MPa site B is just entering tensile failure. At 6.3  
 302 MPa site A is safe. In order to compare the predicted maximum possible overpressure with the Tier 3  
 303 empirical predictions it is necessary to find the overpressure at which the site A would start to fail,  
 304 this is expressed under the row “Site A limit” in Table 7

305 **Table 7 Overpressures simulated and safety margin for model with closed flow boundary at base.**

	Over Pressure prediction from 3D model with closed basal flow boundary.	Over Pressure simulated in 2D model	Maximum fluid pressure to horizontal stress ratio in Reservoir // Primary Seal contact	Minimum factor of Safety in base of Primary Seal
Site A	5.8 MPa	6.3 MPa	0.78	1.64
Site A limit		11.0 MPa	0.96	1.58
Site B	6.0 MPa	6.6 MPa	0.97	1.27

306

307 The Tier (3) empirical model results ( $P_{f\_static}$ ) is an empirical approximation of the Tier (2) “perfect”  
 308 analytical solution, and acts as a reference value against which the dynamic case with heterogeneity,  
 309 geometrical variations and thermal stress influence can be compared. Table 8 presents the  
 310 maximum pressure predictions of Tier (3) empirical model ( $P_{f\_static}$ ) and the Tier (4) THM models of  
 311 the sites A and B. The ratio of the models values of  $P_{f\_static}$  to the THM models are 1:0.63 and 1:0.61  
 312 respectively. From this the maximum dynamic overpressure  $P_{f\_dynamic}$  for the primary seal and  
 313  $P_{f\_dynamic}$  for the secondary seal and faults is given by multiplying these values of  $P_{f\_static}$  from  
 314 equations (21) and (22) respectively by 0.6.

$$315 \quad P_{f\_dynamic} = P_{f\_static} \times 0.6 \quad (40)$$

316 **Table 8 Comparison of static, THM and lookup function values for Site A and B for the primary seal**

	$P_{f\_static}$	THM dynamic model prediction	$P_{f\_dynamic}$
Site A	10.4 MPa	6.6 MPa	6.24 MPa
Site B	18.0 MPa	11.0 MPa	10.8 MPa

317  
 318  $P_{f\_dynamic}$  is now exported as a simple look up function which can be used to estimate the maximum  
 319 overpressure possible within the storage strata under dynamic stress conditions for the primary  
 320 seals, the secondary seal and the faults. The pressures predicted for key strata locations at Site A and  
 321 Site B are presented in Table 9, and illustrated for the whole profile in Figure 6. Also on this figure is  
 322 a commonly used simplified estimate of the maximum possible fluid overpressure presented as 1.3 x  
 323 hydrostatic pressure. Whilst the hydrostatic approach provides a reasonable estimate down to about  
 324 1800 metres, below this it underestimates the amount of possible overpressure.

325 **Table 9 Maximum injection overpressure (OP) values at injection sites after correction for thermal stress and fluid**  
 326 **pressure for the primary seal.**

	Site A		Site B	
	Depth	Max OP	Depth	Max OP
Primary Seal Base	2523 m	10.8 MPa	1912 m	6.24 MPa
Primary Seal Top	2304 m	9 MPa	1727 m	4.98 MPa
Base Secondary Seal	2304 m	4.38 MPa	1727 m	0.96 MPa
Faulting to Reservoir	2523 m	6.36 MPa	1912 m	1.8 MPa

327  
 328 In this case the thermal stress has been shown not to have a significant impact on the safety, and it  
 329 is accommodated in the factor 0.6. However where there is a significant impact this factor can be  
 330 revised in the vicinity of the boreholes. Where faulting is known to extend to the reservoir than the  
 331 secondary seal and faulting values should be applied.

### 332 **Discussion of the application of the four tier approach and application to other** 333 **storage complexes.**

334 The key simplification and advantage of this methodology is to be able to express all the complex  
 335 geomechanical calculations including expected heterogeneity and stress superposition as an  
 336 empirical multivariate expression which acts as a look up function for determining the overpressure  
 337 a strata can withstand. This enables easy application by other users.

338 The application of the geomechanical facies concept for Tier (1) is relatively new, but covered in the  
 339 literature. It provides a fundamental building block to understanding the behavior of any storage

340 complex. The analytical solutions used for Tier (2) are well established and found in any rock  
341 mechanics text book. The use of a multivariate function to approximate the results of Tier (2)  
342 analysis throughout the storage complex and provide the Tier (3) approximation under static stress  
343 conditions has not been done before to the author's knowledge. Combining the Tier (3) modelling  
344 with fully coupled THM simulations Tier (4) to develop a look up function for dynamic stress  
345 conditions is new. Static stress can be mapped to dynamic stress conditions using a relatively simple  
346 formula, and so the stability under dynamic stress conditions can be expected to behave similarly to  
347 the stability under static conditions. The heterogeneity expected within the profile and the impact of  
348 thermal stress is then taken into account by comparing the numerical solution results with the Tier  
349 (3) results and augmenting the Tier (3) results with a factor to account for the dynamic stress  
350 conditions and heterogeneity.

351 Like any other geomechanical analysis the methodology requires that the stress profile is well  
352 known. The analytical solution in Tier (2) if it is only depth dependent assumes lateral stress  
353 consistency, and no significant changes due to thermal stress. Where this is not the case then the  
354 stability estimation will be inaccurate. However the better a regional profile is known the more  
355 accurate the predictions will be. In the case concerned it was clear that regionally the stress profile  
356 suggested an increase in gradient around about the commencement of the chalk group. An  
357 improvement on the analytical function could be the inclusion of the discrete depth of the chalk  
358 group. Extending this to other situation means that a good understanding of the stress profile as a  
359 function of the geomechanical facies could improve the accuracy of the results.

360 The empirical fitting of the analytical function is a further source of uncertainty. Empirical functions  
361 will tend to provide better fits in some areas of the data set than in other areas. Care needs to be  
362 taken that the depths represented within the storage complex are fitted adequately.

363 During the dynamic modelling, the larger scale heterogeneities can be taken into account, however  
364 although the grid scale can be of the order of 10 m or less, the data is provided typically with a  
365 horizontal accuracy at the best of 250 m and a vertical accuracy of the order of 1 m in the boreholes.  
366 Statistical interpretation can be used to "fill in the gaps", however they remain approximations of  
367 the system, and the results cannot be considered as a unique solution. This suggests caution in over  
368 stating the accuracy of the modelling results, and introduces realism into the accuracy of possible  
369 numerical simulations. In addition the parametrization of such large multi process models relies on  
370 laboratory, field and at time literature values, all of which carry differing degrees of uncertainty.

371 Taking into account the possible inaccuracies within the modelling approach, the predictions of the  
372 combinations of the modelling approaches (Tier 3 with a dynamic stress correction vs THM  
373 numerical model) are shown to be remarkably similar for two different sites, with different  
374 geometry and operational conditions. Therefore this methodology enabling the application of an  
375 empirical function based on an analytical evaluation of the static stress profile and a correction to  
376 account for the dynamic stress conditions and heterogeneity can be seen to provide a reasonable  
377 estimate of the geomechanical stability of the storage strata.

378 Further work could include the simulation of several further sections in the storage complex  
379 depending on the data available, in an attempt to improve the validity of the of the approach for  
380 deeper and shallower systems.

381

## 382 **Summary of key modelling results**

383 The following points provide a summary of the key findings of the modelling work

- 384 • The underburden contributes to the amount of pore space available to dissipate the increased pressure  
385 due to CO<sub>2</sub> injected into the reservoir
- 386 • The characteristics of the basal flow boundary and the nature of the Underburden have a very

387 significant impact on the regional development of a pressure signal due to CO<sub>2</sub> injection, and on the  
388 pressure connectivity of multiple sites

- 389 • The stability of the strata is related to the local stress field. The local stress field is dependent upon  
390 stress bridging effects caused by the material properties of the various strata. In the Captain Sandstone  
391 Fairway the depth of the Cretaceous Chalk defines a change in the rate of increase in the horizontal  
392 stress profile.
- 393 • Redistribution of regional stress due to overprint of thermal stress may in some situations increase the  
394 stability of the storage complex.
- 395 • As deeper reservoirs can maintain higher overpressures than shallow reservoirs, care needs to be taken  
396 in designing a multi-user store that the overall pressure signal does not compromise the safety of  
397 shallower areas of the reservoir due to pressure migration from the from deeper areas of the formation.
- 398 • The results of the analytical static stress modelling approach and the numerical dynamic stress  
399 modelling approach presented using an empirical function providing regional coverage of the storage  
400 asset and including implicitly all the complexity of the numerical heterogeneous calculations.

## 401 Conclusions

402 There will be an increased drive for the creation of large shared regional multi-user CO<sub>2</sub> storage  
403 assets in the near future as a technology to reduce CO<sub>2</sub> emissions to the atmosphere. Screening of  
404 complex stratigraphic stores will be necessary to predict and assess the integrity of existing and  
405 planned storage operations. One of the key factors which determine the integrity of a multi-user  
406 store is its geomechanical stability. The cumulative result of multiple CO<sub>2</sub> injection sites is that fluid  
407 pressure from different locations will be superimposed on one another.

408 Using a geomechanical facies approach, this paper has shown how analytical geomechanical models,  
409 empirical assumptions and numerical models can be combined to provide a simple but powerful tool  
410 for the prediction of the maximum overpressure possible in various strata, within fault systems and  
411 with a thermal stress overprint.

412 In addition the numerical modelling of the Captain Sandstone Fairway has highlighted the  
413 importance of including the Underburden in the fluid pressure calculations, both in terms of the  
414 nature of the basal boundary to flow, in providing access to additional pore space for storage, and as  
415 a major control in the regional pressure connectivity between injection sites.

416 The change in the stress field as a result of superposition of pore pressure within the reservoir and  
417 the thermal stress is dependent on the heterogeneity of the strata present. The distribution of fluid  
418 flow is dominated by the heterogeneity in permeability of different layers, which can easily be  
419 several orders of magnitude in difference. The mechanical parameters exhibit one or two orders of  
420 magnitude difference, where as the thermal parameters are all of the same magnitude. The thermal  
421 plume after injection for circa 30 years does not extend significantly beyond 500 metres from the  
422 injecting well, where as the fluid pressure field extends over several tens of kilometres. The nature  
423 of the strata overlying the injection point and underlying the injection well determines the response  
424 of the system to the combination of thermal stress and fluid pressure. Stress bridging can, in some  
425 cases, lead to enhanced stability in sealing rock layers as this redistributes the horizontal stress.

426 In a regionally extensive reservoir, as deeper parts of the reservoir can maintain higher overpressure  
427 values than shallower parts, care needs to be taken to design and manage a multi-user store so that  
428 the overall pressure signal does not compromise the integrity of a shallower store due to pressure  
429 migration from the from deeper strata. This leads to an interesting challenge to manage and  
430 optimise the time dependent pressure footprint of different injection sites.

431 The results of the analytical static stress modelling approach and the numerical dynamic stress  
432 modelling approach presented using an empirical function providing regional coverage of the  
433 storage asset and included implicitly all the complexity of the numerical heterogeneous calculations.  
434 This methodology significantly simplifies the evaluation of the geomechanical stability of extensive  
435 regional CO<sub>2</sub> storage assets.

436

## 437 Acknowledgements

438 The research leading to these results was conducted within the context of the CO2MultiStore project  
439 supported by and published with the permission of the Scottish Government, The Crown Estate,  
440 Scottish Enterprise, Shell and Vattenfall. It was also conducted within the context of the European  
441 Community's Seventh framework Programme FP7/2007-2013 under the grant agreement No.  
442 282900 as part of the PANACEA project.

## 443 References

- 444 CAPPAS, F., AND RUTQVIST, J., 2011, Modeling of coupled deformation and permeability evolution during  
445 fault reactivation induced by deep underground injection of CO<sub>2</sub>: *International Journal of*  
446 *Greenhouse Gas Control*, v. 5, p. 336-346.
- 447 CHANG, C., ZOBACK, M.D., AND KHAKSAR, A., 2006, Empirical relations between rock strength and  
448 physical properties in sedimentary rocks: *Journal of Petroleum Science and Engineering*, v.  
449 51, p. 223-237.
- 450 DECC, 2013. Preferred bidders announced in UK's £1bn CCS Competition. Press release 13/028, 20  
451 March 2013, UK Department of Energy & Climate Change Available at:  
452 [https://www.gov.uk/government/news/preferred-bidders-announced-in-uk-s-1bn-ccs-](https://www.gov.uk/government/news/preferred-bidders-announced-in-uk-s-1bn-ccs-competition)  
453 [competition](https://www.gov.uk/government/news/preferred-bidders-announced-in-uk-s-1bn-ccs-competition)
- 454 DE MARSILY, G. D., 1986, *Quantitative hydrogeology : groundwater hydrology for engineers / Ghislain*  
455 *de Marsily*; translated by Gunilla de Marsily, San Diego, Calif. ; London : Academic Press
- 456 EDLMANN, K., EDWARDS, M.A., QIAO, X.J., HASZELDINE, R.S., AND MCDERMOTT, C.I., 2014, Appraisal of global  
457 CO<sub>2</sub> storage opportunities using the geomechanical facies approach: *Environmental Earth*  
458 *Sciences*, p. 1-22.
- 459 EU, 2011. Implementation of Directive 2009/31/EC on the geological storage of carbon dioxide –  
460 Guidance Document 2 – Characterisation of the storage complex, CO<sub>2</sub> stream composition,  
461 monitoring and corrective measures.
- 462 FJAER, E., HOLT, R.M., HORSRUD, P., RAAEN, A. M. AND RISNES, R. 2008. *Petroleum related rock mechanics*,  
463 *Second Edition*, Hungary: Elsevier Science Ltd. ISBN 978-0-444-50260-5, p491
- 464 GEUZAIN, C., AND REMACLE, J.-F., 2009, Gmsh: A 3-D finite element mesh generator with built-in pre-  
465 and post-processing facilities: *International Journal for Numerical Methods in Engineering*, v.  
466 79, p. 1309-1331.
- 467 HILLIS, R.R., 2001, Coupled changes in pore pressure and stress in oil fields and sedimentary basins:  
468 *Petroleum Geoscience*, v. 7, p. 419-425.
- 469 JAEGER, J., COOK, N., AND ZIMMERMAN, R., 2007, *Fundamentals of rock mechanics 4th edition*, Malden,  
470 USA: Blackwell Publishing Ltd.
- 471 JOHNSON, H., AND LOTT, G. K., 1993, 2. Cretaceous of the Central and Northern North Sea. in  
472 *Lithostratigraphic nomenclature of the UK North Sea*. KNOX, R W O'B. and CORDEY, W G.  
473 (editors). British Geological Survey, Nottingham.
- 474 KIM, S., AND HOSSEINI, S.A., 2014, Geological CO<sub>2</sub> storage: Incorporation of pore-pressure/stress  
475 coupling and thermal effects to determine maximum sustainable pressure limit: *Energy*  
476 *Procedia*, v. 63, p. 3339-3346.
- 477 KNOX, R. W. O'B., AND HOLLOWAY, S., 1992, 1. Paleogene of the Central and Northern North Sea. in  
478 *Lithostratigraphic nomenclature of the UK North Sea*. KNOX, R W O'B. and CORDEY, W G.  
479 (editors). British Geological Survey, Nottingham.
- 480 KOLDITZ, O., BAUER, S., BILKE, L., BÖTTCHER, N., DELFS, J.O., FISCHER, T., GÖRKE, U.J., KALBACHER, T.,  
481 KOSAKOWSKI, G., MCDERMOTT, C.I., PARK, C.H., RADU, F., RINK, K., SHAO, H., SHAO, H.B., SUN, F.,  
482 SUN, Y.Y., SINGH, A.K., TARON, J., WALTHER, M., WANG, W., WATANABE, N., WU, Y., XIE, M., XU, W.,  
483 AND ZEHNER, B., 2012, OpenGeoSys: An open-source initiative for numerical simulation of

484 thermo-hydro-mechanical/chemical (THM/C) processes in porous media: Environmental  
485 Earth Sciences, v. 67, p. 589-599.

486 KOLDITZ, O., GÖRKE, U.-J., SHAO, H., AND WANG, W., 2012, Thermo-hydro-mechanical-chemical processes  
487 in porous media: benchmarks and examples, Springer Science & Business Media, ISBN 978-3-  
488 642-27176-2, pp 391

489 LEWIS, R.W., AND SCHREFLER, B.A., 1998, The Finite Element Method in the Static and Dynamic  
490 Deformation and Consolidation of Porous Media: Chichester, England, John Wiley & Sons,  
491 492 p.

492 MAGRI, F., TILLNER, E., WANG, W., WATANABE, N., ZIMMERMANN, G., AND KEMPKA, T., 2013, 3D Hydro-  
493 mechanical Scenario Analysis to Evaluate Changes of the Recent Stress Field as a Result of  
494 Geological CO2 Storage: Energy Procedia, v. 40, p. 375-383.

495 McDERMOTT, C.I., LODEMANN, M., GHERGUT, I., TENZER, H., SAUTER, M., AND KOLDITZ, O., 2006a,  
496 Investigation of coupled hydraulic-geomechanical processes at the KTB site: Pressure-  
497 dependent characteristics of a long-term pump test and elastic interpretation using a  
498 geomechanical facies model: Geofluids, v. 6, p. 67-81.

499 McDERMOTT, C.I., RANDRIAMANJATOSOA, A.R.L., TENZER, H., AND KOLDITZ, O., 2006b, Simulation of heat  
500 extraction from crystalline rocks: The influence of coupled processes on differential reservoir  
501 cooling: Geothermics, v. 35, p. 321-344.

502 PINNOCK, S.J., CLITHEROE, A.R.J., AND ROSE, P.T.S., 2003, The Captian Field, Block 13/22a, UK North Sea,  
503 *in* Gluyas, J.G.H., H.M., ed., United Kingdom Oil and Gas Fields, Commemorative Millennium  
504 Volume, Geological Society, London, Memoir, p. 431-441.

505 RUTQVIST, J., BIRKHOLZER, J., CAPPA, F., AND TSANG, C.F., 2006, Estimating maximum sustainable injection  
506 pressure during geological sequestration of CO2 using coupled fluid flow and geomechanical  
507 fault-slip analysis.

508 RUTQVIST, J., WU, Y.S., TSANG, C.F., AND BODVARSSON, G., 2002, A modeling approach for analysis of  
509 coupled multiphase fluid flow, heat transfer, and deformation in fractured porous rock:  
510 International Journal of Rock Mechanics and Mining Sciences, v. 39, p. 429-442.

511 SCCS, 2011. Progressing Scotland's CO2 Storage opportunities, 60pp. Available at:  
512 [http://www.sccs.org.uk/images/expertise/reports/progressing-scotlands-](http://www.sccs.org.uk/images/expertise/reports/progressing-scotlands-co2/ProgressingScotlandCO2Opps.pdf)  
513 [co2/ProgressingScotlandCO2Opps.pdf](http://www.sccs.org.uk/images/expertise/reports/progressing-scotlands-co2/ProgressingScotlandCO2Opps.pdf)

514 SCCS, 2015. Optimising CO2 storage in geological formations; a case study offshore Scotland,  
515 CO2MultiStore project. Scottish Centre for Carbon Storage Report, 76pp. ISBN: 978-085272-  
516 852-9 Available at: <http://www.sccs.org.uk/images/expertise/reports/>

517 SHELL 2011A. GEOMECHANICS SUMMARY REPORT. SCOTTISHPOWER CCS CONSORTIUM, UK CARBON CAPTURE AND  
518 STORAGE COMPETITION REPORT , UK CCS-KT-S7.19-SHELL-004, p.104

519 SHELL 2011B. PORE PRESSURE PREDICTION. SCOTTISHPOWER CCS CONSORTIUM, UK CARBON CAPTURE AND  
520 STORAGE COMPETITION REPORT , UK CCS-KT-S7.21-SHELL-006, p.30

521 SHELL 2011C. STATIC MODEL (AQUIFER). SCOTTISHPOWER CCS CONSORTIUM, UK CARBON CAPTURE AND STORAGE  
522 COMPETITION REPORT , UK CCS-KT-S7.22-SHELL-001, p.37

523 TENZER, H., PARK, C.H., KOLDITZ, O., AND McDERMOTT, C.I., 2010, Application of the geomechanical facies  
524 approach and comparison of exploration and evaluation methods used at Soultz-sous-Forêts  
525 (France) and Spa Urach (Germany) geothermal sites: Environmental Earth Sciences, v. 61, p.  
526 853-880.

527 VIDAL-GILBERT, S., NAUROY, J.-F., AND BROSSE, E., 2009, 3D geomechanical modelling for CO2 geologic  
528 storage in the Dogger carbonates of the Paris Basin: International Journal of Greenhouse Gas  
529 Control, v. 3, p. 288-299.

530 WILLIAMS, J., KIRK, K., AND MONAGHAN, A., 2013, Task 2.1 CO2MultiStore - Static geological model of the  
531 Captain Sandstone, risk reduction and knowledge exchange., British Geological Survey  
532 Internal Report., p. 61pp.

533 ZIENKIEWICZ, O.C., AND TAYLOR, R.L., 2005, The Finite Element Method, v. 1, Butterworth Heinemann,  
534 752 p.

